

**Spatial source contribution and interannual variation in
deposition of dust aerosols over the Chinese Loess
Plateau**

Ove Haugvaldstad^{1,3}, Hui Tang^{1,2,5}, Anu Kaakinen², Christine D. Groot Zwaafink⁶, Henrik Grythe⁶, Katja Bohm^{2,4}, Thomas Stevens^{4,2}, Zhongshi Zhang⁷, Frode Stordal¹

¹Department of Geosciences, University of Oslo, Norway

²Department of Geosciences and Geography, University of Helsinki, Finland

³Norwegian Meteorological Institute, Oslo, Norway

⁴Department of Earth Sciences, Uppsala University, Sweden

⁵Finnish Meteorological Institute (FMI), Climate System Research, Helsinki, Finland

⁶Norwegian Institute for Air Research, Kjeller, Norway.

⁷Department of Atmospheric Science, School of Environmental studies, China University of Geoscience, 430074 Wuhan, China.

Key Points:

- The source contribution of emitted dust aerosols to the Chinese Loess Plateau (CLP) is mapped using backward trajectory modeling.
- Distant dust emission regions in Central Asia have a non-negligible impact on the CLP, with wet-deposited dust showing a clearer connection.
- Strong dust deposition years over the CLP are associated with the negative phase of the Arctic Oscillation.

Abstract

The Chinese Loess Plateau (CLP) in northern China serves one of the most prominent loess records in the world. The CLP is an extensive record of changes in past aeolian dust activity in East Asia; however, the interpretation of the loess records is hampered by ambiguity regarding the origin of loess-forming dust and an incomplete understanding of the circulation forcing dust accumulation. In this study, we used a novel modeling approach combining a dust emission model FLEXDUST with simulated back trajectories from FLEXPART to trace the dust back to where it was emitted. Over 21 years (1999-2019), we modeled back trajectories for fine ($\sim 2 \mu\text{m}$) and super-coarse ($\sim 20 \mu\text{m}$) dust particles at six CLP sites during the peak dust storm season from March to May. The source receptor relationship from FLEXPART is combined with the dust emission inventory from FLEXDUST to create site-dependent high-resolution maps of the source contribution of deposited dust. The nearby dust-emission areas dominate the source contribution at all sites. Wet deposition is important for dust deposition at all sites, regardless of dust size. Non-negligible amounts of dust from distant emission regions could be wet deposited on the CLP following high-level tropospheric transport, with the super-coarse dust preferentially from emission areas upwind of sloping topography. On an interannual scale, the phase of the Arctic Oscillation (AO) in winter was found to have a strong impact on the deposition rate on the CLP, while the strength of the East Asian Winter Monsoon was less influential.

Plain Language Summary

The dust deposits on the Chinese Loess Plateau (CLP) in northern China provide an extensive record of changes in past dust activity in East Asia. In this work, we combine an atmosphere transport model with a dust emission model to trace the dust backward to where it was emitted. Choosing six locations at the CLP where we trace the dust back to emissions over a 21-year period during the most active dust months from March until May, for which we investigated how different parts of the CLP were influenced by the different dust emission areas, transport mechanisms, and wind circulation patterns. We find that dust is mainly brought from the emissions areas located near the CLP, still dust from far-away emissions areas in Central Asia has the potential to reach the CLP in smaller amounts. Furthermore, our results show that wet removal of dust by precipitation is important for dust deposition on the CLP, a mechanism that is often overlooked when explaining variations in past dust activity. On a year-to-year basis the dust deposition rate over the CLP was found to be connected to the high-latitude northern hemisphere's climate oscillation (Arctic Oscillation) rather than the regional East Asian winter monsoon.

1 Introduction

Mineral dust is deeply embedded within the Earth system, influencing the planet's energy balance, cloud characteristics, atmospheric chemistry, and biogeochemistry (Shao et al., 2011; Kok et al., 2023). Dust is mainly emitted from dry and sparsely vegetated arid and semi-arid regions. Emission is driven by surface winds that lift sand grains from the soil bed, where the impact upon reentry ejects and fragments smaller soil particles, which then get transported. The dust-emitting capacity of the soil is strongly influenced by environmental factors such as soil moisture, vegetation, soil texture, and the structure of the top soil. On geological time scales, dust depositional records show increases in dust activity during glacial periods (Porter, 2001; Maher, 2016). However, as human expansion has increased the intensification of land use in recent years, we are now seeing a profound impact of human activity on dust activity, e.g. the drying of Aral Sea and dust bowl in the 1930s

72 North America. The anthropogenic signal is also evident in the depositional records,
 73 which show that in the last 150 years there has been an increase in the dust burden
 74 globally of about 50% (Hooper & Marx, 2018). However, we do not know to what
 75 extent this is due to a forcing caused by increased human activity and changes in
 76 land use in semi-arid regions or to modifications in precipitation and wind patterns
 77 in a changing climate (Kok et al., 2023).

78 Changes in dust activity are important because of the climate effect of dust.
 79 Fine dust aerosols exerts cooling effect due to its ability to reflect incoming sun-
 80 light , whereas coarse dust aerosols cause a warming effect as they interact with the
 81 outgoing long-wave radiation. Furthermore, different dust-emitting regions have dif-
 82 ferent dust mineralogy, which affects its ability to absorb radiation (Dubovik et al.,
 83 2002). Atmospheric dust particles also affect clouds by acting as nuclei for condens-
 84 ation, contributing to droplet formation. Additionally, dust particles act as nuclei
 85 to initiate glaciation of clouds above the temperatures of homogeneous freezing. Ice
 86 clouds generally have a warming effect, whereas liquid clouds have a cooling effect
 87 (Storelvmo, 2017). The deposition of dust on snow accelerates snow melt (Wittmann
 88 et al., 2017; Sarangi et al., 2020), while dust input can increase ecosystem produc-
 89 tivity in regions lacking nutrients, by providing iron or phosphorus (Martin, 1990;
 90 Yu et al., 2015). These processes impact the climate system, but the complexities
 91 introduced by the poor constraints of, for example, dust particle size (A. Adebiyi et
 92 al., 2023; Ryder et al., 2018), shape (Huang et al., 2020), mineralogical composi-
 93 tion (Li et al., 2021) and dust-cloud interactions (Sagoo & Storelvmo, 2017) of air-
 94 borne dust particles, make the overall climatic effect of the dust uncertain (Kok et
 95 al., 2023).

96 One of the most prominent dust records on Earth for studying environmen-
 97 tal drivers of changes in the dust cycle is the Chinese Loess Plateau (CLP), located
 98 in the north central part of China (Figure 1). Here windblown dust has been ac-
 99 cumulating since at least the late Oligocene-early Miocene (c. 25-22 Ma) (Guo et
 100 al., 2002; Qiang et al., 2011), providing a long-term, nearly continuous record of
 101 past responses of the East Asian Dust Cycle (EADC) to environmental and climatic
 102 changes (e.g. Stevens et al., 2007; Lu et al., 2010; Maher, 2016; Y. Sun et al., 2020).

103 The sediment sources, dust-emitting regions, transportation, and deposition
 104 processes of the eolian deposits on the CLP are debated (e.g. W. Peng et al., 2023;
 105 H. Zhang et al., 2022; Shang et al., 2016; Bird et al., 2015; D. Sun et al., 2008).
 106 However, most agree that the dust was generally sourced from the dry Asian inter-
 107 ior and proximal deserts via energetic, surface-level northwesterly winds driven by
 108 the East Asian Winter Monsoon (EAWM) system (Z. Ding et al., 1999). In addition
 109 to the EAWM, the prevailing mid-latitude westerlies in the middle and upper tro-
 110 posphere play an important role in transporting dust to the CLP. The EAWM and
 111 the westerlies are suggested to explain the bimodal particle size distribution widely
 112 observed in the CLP records. The coarse particles are suggested to be transported
 113 by the strong surface winds associated with the EAWM and the fine particles are
 114 suggested to represent the background dust component of the CLP transported by
 115 the high-level westerly air flow (Miao et al., 2004; D. Sun, 2004; D. Sun et al., 2008).
 116 Furthermore, both the particle size distribution and the dust accumulation of the
 117 loess records exhibit a northwest-southeast gradient (Z. Ding et al., 1999), which fur-
 118 ther supports the northwesterly and westerly wind driven transport pathways.

119 Recent studies using single grain provenance indicators on the CLP dust records
 120 shed more light on dust emission areas and transport pathways, and their variation
 121 in the geologic past (Bird et al., 2015; Shang et al., 2016; Nie et al., 2018; H. Zhang
 122 et al., 2021, 2022; Bohm et al., 2023; W. Peng et al., 2023). However, the interpreta-
 123 tion of the CLP provenance records is hampered by the complexity of the source-to-
 124 sink system and by the fact that dust provenance signals reflect not only the trans-

125 porting wind systems, but also the various processes that affect dust availability in
 126 the source regions. Furthermore, single grain provenance ultimately tells us what
 127 the source rocks and sediments are, which might be different from the dust-emitting
 128 regions.

129 Several provenance studies have reported spatial provenance differences across
 130 the CLP for both Neogene Red Clay and Quaternary loess (e.g. Bird et al., 2015;
 131 Shang et al., 2016; H. Zhang et al., 2021; W. Peng et al., 2023). However, the cause
 132 of the spatial differences in provenance is not well established. The Yellow River
 133 has been argued to cause these spatial differences by bringing material from the
 134 Northern Tibetan Plateau closer to the CLP before the final aeolian transport step
 135 (Stevens et al., 2013; Nie et al., 2015). Contrasting eolian dust transport pathways
 136 for different parts of the CLP have also been proposed to add to the spatial dif-
 137 ference (Shang et al., 2016), with the northern and northeastern parts of the CLP
 138 dominated by dust from the northwestern deserts via the EAWM, and the south-
 139 ern and southwestern parts of the CLP dominated by dust from the Northern Ti-
 140 betan Plateau and even the remote Taklamakan desert via the westerlies (Shang et
 141 al., 2016).

142 Applications of the provenance method to further unravel the dust cycle over
 143 the CLP is also hampered by the fact that most single grain provenance approaches
 144 are based on a relatively large particle size ($> 20 \mu\text{m}$). Our understanding of the
 145 transport of such large dust particles in the atmosphere is still limited and highly
 146 debated (A. Adebiyi et al., 2023). Super-coarse dust particles (sensu A. Adebiyi et
 147 al. (2023), $> 20\mu\text{m}$) have commonly been assumed to be transported only a short
 148 distance (1-100 km) from the source region because of the high gravitational settling
 149 velocity (Tsoar & Pye, 1987), which contradicts CLP provenance inferences of dust
 150 derived from remote deserts, such as the Taklamakan. Furthermore, recent observa-
 151 tions have documented the possibility of long-distance transportation ($> 1000 \text{ km}$) of
 152 giant ($> 62.5\mu\text{m}$) dust particles (Van Der Does et al., 2018; Varga et al., 2021). A
 153 better understanding of large dust particle transportation to the CLP will help the
 154 interpretation of dust provenance proxies, and thus improve our understanding of
 155 the EADC on geological time scales.

156 Dust models have been widely applied to understand the EADC, however,
 157 there have been only limited cases where dust models have been applied to under-
 158 stand the formation of the CLP dust records in particular (Shi & Liu, 2011). More-
 159 over, previous modeling studies of past and present EADC have typically applied
 160 global or regional climate models (Shi & Liu, 2011; S. L. Gong et al., 2006), which
 161 mainly consider particles within the fine to coarse range ($< 10\mu\text{m}$) (Zhao et al.,
 162 2022). These models are also unable to determine the exact sources of emitted dust
 163 for different locations at the CLP, which would greatly enhance the provenance in-
 164 terpretations of the CLP dust records. To address these issues, we used the La-
 165 grangian particle dispersion model FLEXPART. We run FLEXPART backward in a
 166 receptor-oriented viewpoint, which, paired with a dust emission field, allows us to es-
 167 tablish high-resolution source contribution maps. We apply FLEXPART to establish
 168 source receptor relationships between six loess sites across the CLP and examine the
 169 interannual variations in deposition at these over a 20-year period from 1999-2019.
 170 In this study, both fine ($1.7\text{-}2.5 \mu\text{m}$) and super-coarse ($15\text{-}20 \mu\text{m}$) dust particles are
 171 simulated to better understand whether the deposition of fine particles occurs under
 172 the same climate conditions as that of coarse particles and whether the source re-
 173 gions are the same. We chose to study the interannual variation in the dust deposi-
 174 tion rate over the CLP because we are interested in understanding the processes re-
 175 sponsible for the changes in loess MAR, with implications for identifying the factors
 176 that could be driving the changes that have occurred on longer time scales(F. Peng
 177 et al., 2022).

178 2 Model and Data

179 2.1 FLEXDUST and FLEXPART

FLEXDUST is an offline dust emission model developed to be used in pair with the Lagrangian dispersion model FLEXPART to study the long-range transport and deposition of windblown dust (Groot Zwaftink et al., 2016). The combination FLEXDUST-FLEXPART has previously been applied to study the sources, transport, and deposition of high-latitude dust (Groot Zwaftink et al., 2017; Kylling et al., 2018; Wittmann et al., 2017). The dust emitted in FLEXDUST is assumed to have a volume size distribution between 0.2 and 20 μm according to the brittle fragmentation theory described in Kok (2011). Tang et al. (2023) identified several weaknesses in the way dust-emitting areas in East Asia were represented in the original FLEXDUST version. Therefore, we use the updated version of FLEXDUST by Tang et al. (2023), which includes several changes to better represent present day dust emission areas in East Asia. To avoid confusion with the standard version of FLEXDUST, we refer to the updated Tang et al. (2023) version of FLEXDUST as FLEXDUST-EA. Changes in FLEXDUST-EA compared to FLEXDUST include: (1) the parameterization of vertical dust flux described by Kok et al. (2014) with a modified parameter for the calculation of the threshold friction velocity according to Shao and Lu (2000), (2) the soil texture dataset in the ISRIC SoilGrids dataset described by de Sousa et al. (2020), (3) new improved topographical erodibility scaling, and (4) herbaceous and crop land cover types in the GLC-NMO land cover dataset are considered to have a potential to emit dust in addition to bare ground and sparse vegetation. For a complete description of the changes in FLEXDUST-EA compared to the standard version, see Tang et al. (2023).

Dust transport and deposition are calculated using FLEXPART version 10.4 (Pisso et al., 2019). FLEXPART is an open source model and has been applied to study the transport of a wide range of atmospheric tracers, such as, mineral dust, black carbon, and volcanic ash (Groot Zwaftink et al., 2022, 2016; Choi et al., 2020; Eckhardt et al., 2008). FLEXPART calculates the trajectories of a large number of computational particles that are used to describe the transport and deposition of tracers in the atmosphere. This version of FLEXPART includes the improved wet deposition scheme based on cloud information from the ECWMF input fields (Grythe et al., 2017). In addition, FLEXPART accounts for gravitational settling, dry deposition, and in- and below-cloud scavenging of simulated dust aerosols. Dry deposition is treated using a resistance scheme (Stohl et al., 2005) and in-cloud wet deposition distinguishes between scavenging in the liquid and ice phase (Grythe et al., 2017).

FLEXPART can be run both in forward (source-oriented) and backward (receptor-oriented) mode. The model gives the same results when running in forward or backward mode, except for some minor numerical differences (Seibert & Frank, 2004), and therefore the direction can be set for computational efficiency. Since we are interested in mapping the spatiotemporal contribution of different dust-emitting regions to a receptor, we run FLEXPART in backward mode. In the backward configuration, computational particles are released at a predefined receptor location, and then each particle is traced backward in time. The distribution of the residence time of the computational particles in each grid cell of the output grid is used to calculate the emission sensitivity (ES). ES gives a relationship between a potential source in a grid cell and deposition at the receptor. ES is calculated separately for each dust particle size bin and deposition process. We include two size bins in our FLEXPART simulations, corresponding to fine dust (mean diameter 2 μm) and super-coarse dust (mean diameter 17.6 μm) following the terminology of A. Adebiyi et al. (2023). These two sizes were selected to represent the clay and silt fractions that are typically observed in the Chinese loess. In addition to size, efficiencies for

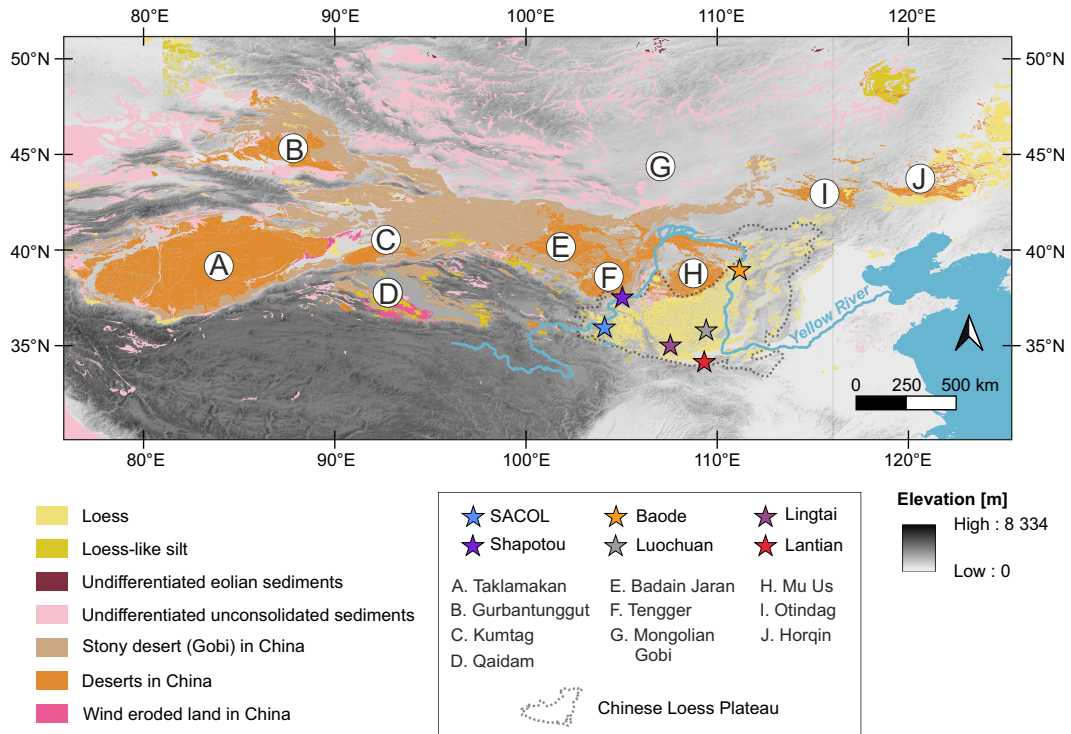


Figure 1. Digital elevation model (Shuttle Radar Topography Mission) and the locations of the Chinese Loess Plateau, the study sites and major dust emitting areas in Central-East Asia. The distribution of loess, loess-like silt, and the undifferentiated sediments are from Börker et al. (2018), and the deserts and wind 477 eroded land in China from 1:200,000 Desert Distribution Dataset provided by the Environmental and Ecological Science Data Center 478 for West China, National Natural Science Foundation of China (<http://westdc.westgis.ac.cn>; last access 27 July 2020).

each of the wet removal processes can be assigned differently depending on the kind of dust-aerosol represented. The parameters we used to represent the two types of airborne dust particles in our FLEXPART simulations are listed in Table 1. Dry deposition ES is calculated by releasing particles from the receptor at the surface level between 0-30 meters and then calculating the particle backtrajectories. Wet deposition ES is calculated by releasing particles throughout the atmospheric column to determine whether a particle is wet scavenged. Then only backtrajectories of the particles that undergo wet scavenging are calculated. Consequently, to achieve a statistically reliable outcome, a greater number of particles are necessary for wet deposition simulations. ES averaged over a selected output layer height can be multiplied by the dust emission inventory (units $\text{kg m}^{-3}\text{s}^{-1}$) created by FLEXDUST, to generate a map that quantifies each contribution of the source element to the deposition at the receptor (Eckhardt et al., 2017). Summing the source contribution (SC) of each source element yields the deposition rate at the receptor.

2.2 FLEXPART backtrajectory set up and workflow

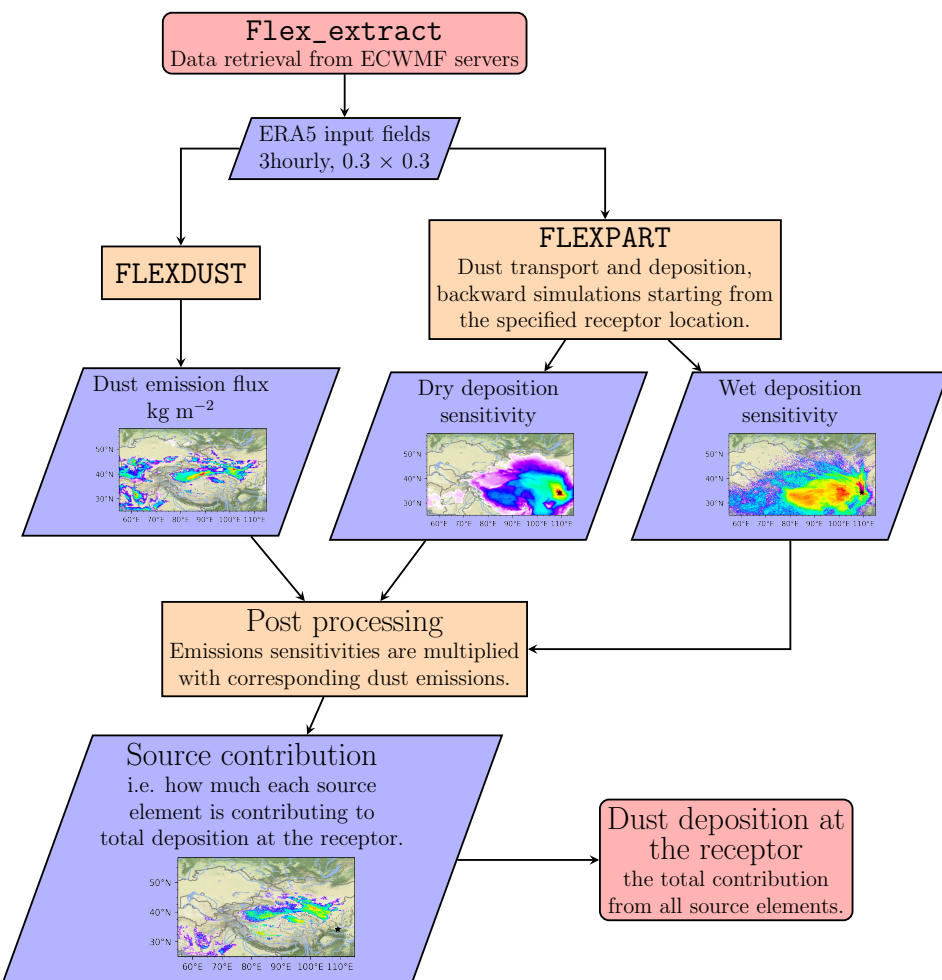


Figure 2. Flow chart showing the workflow for the FLEXPART-FLEXDUST backward trajectory modeling analysis.

246 Backward FLEXPART simulations were performed during the main dust storm
 247 season between March 1st and May 31st over a 21-year period from 1999 until 2019
 248 for six locations across the CLP shown in Figure 1. The selected sites encompassed
 249 both well-established loess sites with historical loess and red-clay deposits (Baode,
 250 Luochuan, Lingtai, and Lantian), as well as modern dust observation sites (Shapotou
 251 and SACOL). This diverse geographical selection of sites allows for a compre-
 252 hensive assessment of dust deposition susceptibility across different parts of the CLP
 253 to different dust emissions regions and circulation patterns.

254 FLEXPART was configured the following way, every particle release contained
 255 either 50,000 or 200,000 particles, depending on whether dry or wet deposition is
 256 simulated. Particles within one release are evenly distributed over 3-hourly inter-
 257 vals. The extent of the backtrajectories was limited to a maximum particle age of
 258 10 days. ES was calculated with 0.1 degree resolution, with an output grid spanning
 259 50-128°longitude, 25-65°latitude, and stored as 3-hourly averages. The FLEXDUST-
 260 EA dust emission flux is multiplied by the averaged ES of 0-100 meters to derive
 261 the deposition source contribution. The parameters of the two particle size bins that
 262 we include are listed in Table 1. We have summarized the stages of the workflow in
 263 Figure 2, commencing with the retrieval and preparation of the forcing data. Then
 264 the calculations of dust emissions, dry and wet dust deposition ES are done concur-
 265 rently. Finally, the FLEXDUST dust emission inventory is combined with FLEX-
 266 PART ES during post-processing to produce the source contribution maps and the
 267 deposition rate for each of the receptor locations.

Table 1. FLEXPART species parameters for the fine and super-coarse dust particle size bins.

	Description	Fine	Super-coarse
PCRAIN_AERO	Efficency of below cloud scavenging by rain (1=100%, 0=off)	1.00	1.00
PCSNOW_AERO	Efficency of below cloud scavenging by snow (1=100%, 0=off)	1.00	1.00
PCC_AERO	CCN efficiency (in cloud scavenging)	0.15	0.30
PIN_AERO	IN efficiency (in cloud scavenging)	0.02	0.10
PDENSITY	Particle density (dry deposition)	2500.0 kg m ⁻³	2500.0 kg m ⁻³
PDQUER	Mean particle diameter (dry deposition)	2.057 μm	17.32 μm
PDSIGMA	Normalized particle diameter deviation	1.21	1.15

268 We used the most recent ECMWF Reanalysis v5 (ERA5) atmospheric forcing
 269 dataset in our FLEXPART and FLEXDUST simulations, the dataset is described in
 270 Hersbach et al. (2020). We used a regional domain cutout of ERA5 extending from
 271 10°E to 160°E and 10°N to 80°N, with a horizontal resolution of 30 km (T639) and
 272 137 vertical levels from the surface up to 0.01 hPa (80 km). ERA5 data were pre-
 273 pared and downloaded from the Copernicus Climate Change Serviced Climate Data
 274 Store using the Flex_extract version 7.0.4 Python package (Tipka et al., 2020). All
 275 ERA5 data are available for free from the Copernicus Climate Data store.

276 2.3 Model evaluation

277 Long-term field observations of dust deposition on the CLP suitable for model
 278 evaluation do not exist. Hence, we have to depend on aerosol reanalysis to assess
 279 the performance of FLEXPART and FLEXDUST-EA. Specifically, we use Modern-
 280 Era Retrospective Analysis for Research and Applications, version 2 (MERRA-2)
 281 aerosol reanalysis produced by NASA's Global Modeling and Assimilation Office

(Gelaro et al., 2017). This dataset has previously been shown reliable at simulating the EADC (H. Liu et al., 2018; W. Yao et al., 2020). Similarly to ERA5, MERRA-2 assimilates essential atmospheric variables such as wind, precipitation, and surface pressure. However, unlike ERA5, MERRA-2 additionally incorporates aerosol optical depth (AOD) retrievals sourced from various ground-based and spaceborne instruments, including the Moderate Resolution Imaging Spectroradiometer (MODIS), the Multiangle Imaging Spectroradiometer (MISR), and the Aerosol Robotic Network (AERONET). Assimilation should bring aerosol loading and AOD in MERRA-2 closer to observations. AOD represents the total aerosol loading but does not provide information on aerosol composition, and therefore the model determines the contribution of dust aerosols to the total AOD. MERRA-2 represent dust aerosols using five size bins (0.1-1.0, 1.0-1.8, 1.8-3.0, 3.0-6.0, and 6.0-10.0 [μm]). Dust emission and deposition are not assimilated in MERRA-2; and are in this regard similar to FLEXDUST relying on the model physics. The wind patterns of MERRA-2 should be similar to those observed in ERA5, however, due to its lower spatial resolution of 0.675 °longitude and 0.5 °latitude, it is not able to capture local-scale winds as accurately as ERA5. This means that MERRA-2 does not necessarily outperform any other dust model (Gelaro et al., 2017; Zhao et al., 2022). For example, Tang et al. (2023) compared FLEXPART for the mega dust storm in spring 2021 with the two most widely used aerosol reanalysis products MERRA-2 and CAMS. The study revealed that FLEXPART exhibited consistency with MERRA-2 with respect to the strength and timing of the event. However, the overall spatio-temporal patterns of total concentration were more in line with CAMS. We still chose to use MERRA-2 as our benchmark because it has a continuous data record dating back to 1980 and covering the entire modeling period of this work.

3 Results and Discussion

3.1 The spatial distribution and interannual variation of the East Asian spring dust cycle

Our setup using FLEXPART coupled with FLEXDUST-EA was developed to represent East Asian sources and Tang et al. (2023) showed that it can realistically simulate the evolution of single dust events, compared to both observations and reanalysis. Here, we evaluated FLEXDUST-EA by comparing it with MERRA-2 over a longer time period. Zamora et al. (2022) have also shown a comparison with MERRA-2 products focusing on the Arctic region, where they found mainly differences based on a lack of high-latitude dust sources in MERRA-2. The spatial distribution of dust emissions in FLEXDUST-EA aligns closely with that of MERRA-2, as illustrated in Figure 3. Both FLEXDUST-EA and MERRA-2 identify key dust emission hot spots in East Asia, including the Taklamakan desert, north-western deserts, and the Gobi desert, which is consistent with previous studies (Kok et al., 2021; Shi & Liu, 2011; Shao & Dong, 2006; J. Sun et al., 2001). Moreover, FLEXDUST-EA shows a strong correlation with MERRA-2 regarding the interannual variation in spring dust emission across all major source regions. Both models show notably lower dust emissions during the springs of 2005 and 2019 and higher emissions during 2001 and 2004. In addition, the period between 1999 and 2009 has greater variability in dust emissions compared to 2010 to 2019 in both FLEXDUST-EA and MERRA-2.

Next, we evaluate how FLEXPART represents the interannual variation of dust deposition at our sites by comparing the springtime dust deposition simulated by FLEXPART with that of the MERRA-2 grid box closest to our sites. Figure 4a shows the interannual variation of the total spring deposition simulated by FLEXPART versus MERRA-2, comparing the fine dust size bin (mean diameter 2 μm) in FLEXPART with the 1.0-1.8 μm size bin in MERRA-2. The models correlate

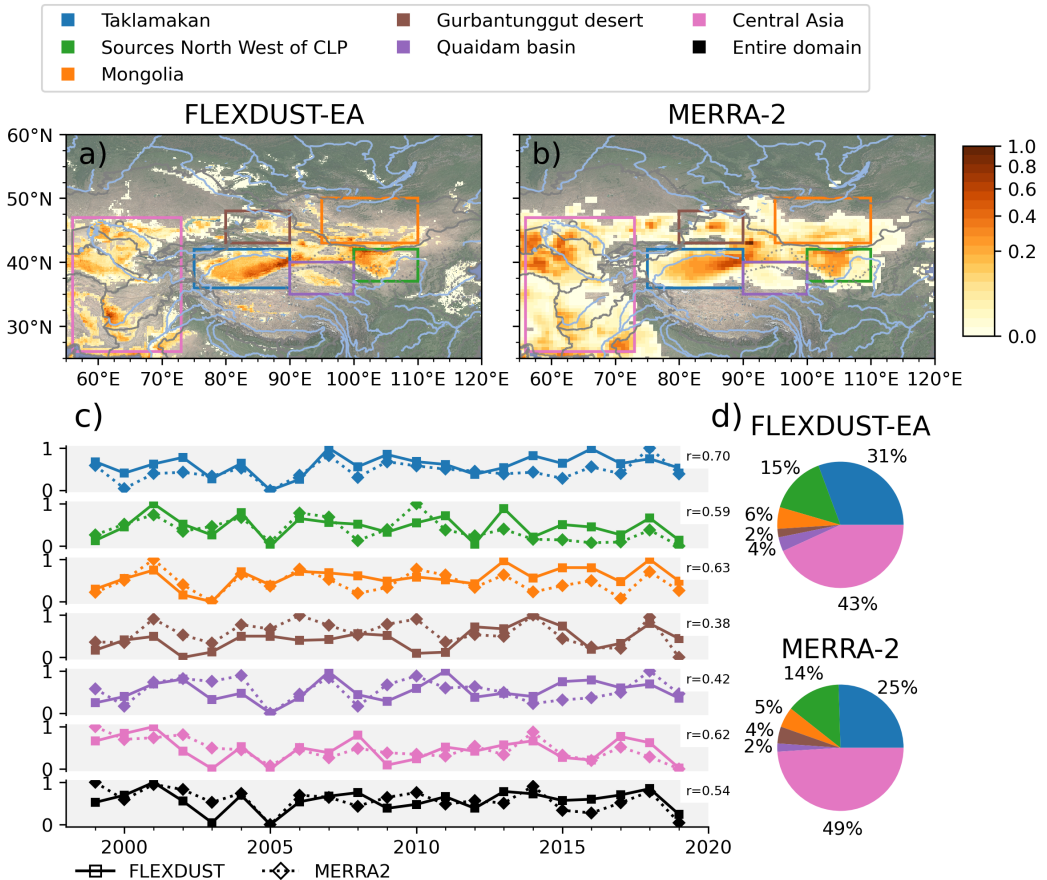


Figure 3. Normalized mean spring dust emissions (a) FLEXDUST and (b) MERRA-2 between 1999 and 2019. The following dust-emitting regions are indicated: Taklamakan (blue, A), Qaidam Basin (purple, D), sources northwest of CLP (green, E,F,H), Mongolia (orange, G,I), Gurbantunggut Desert (brown, B) and Central Asia (pink), the letters correspond to dust emission regions named in Figure 1. (c) Normalized timeseries of spring dust emissions FLEXDUST (solid line) and MERRA2 (dotted line), numbers in the upper right corners show the correlation coefficient. (d) The relative dust emission strength of each source region.

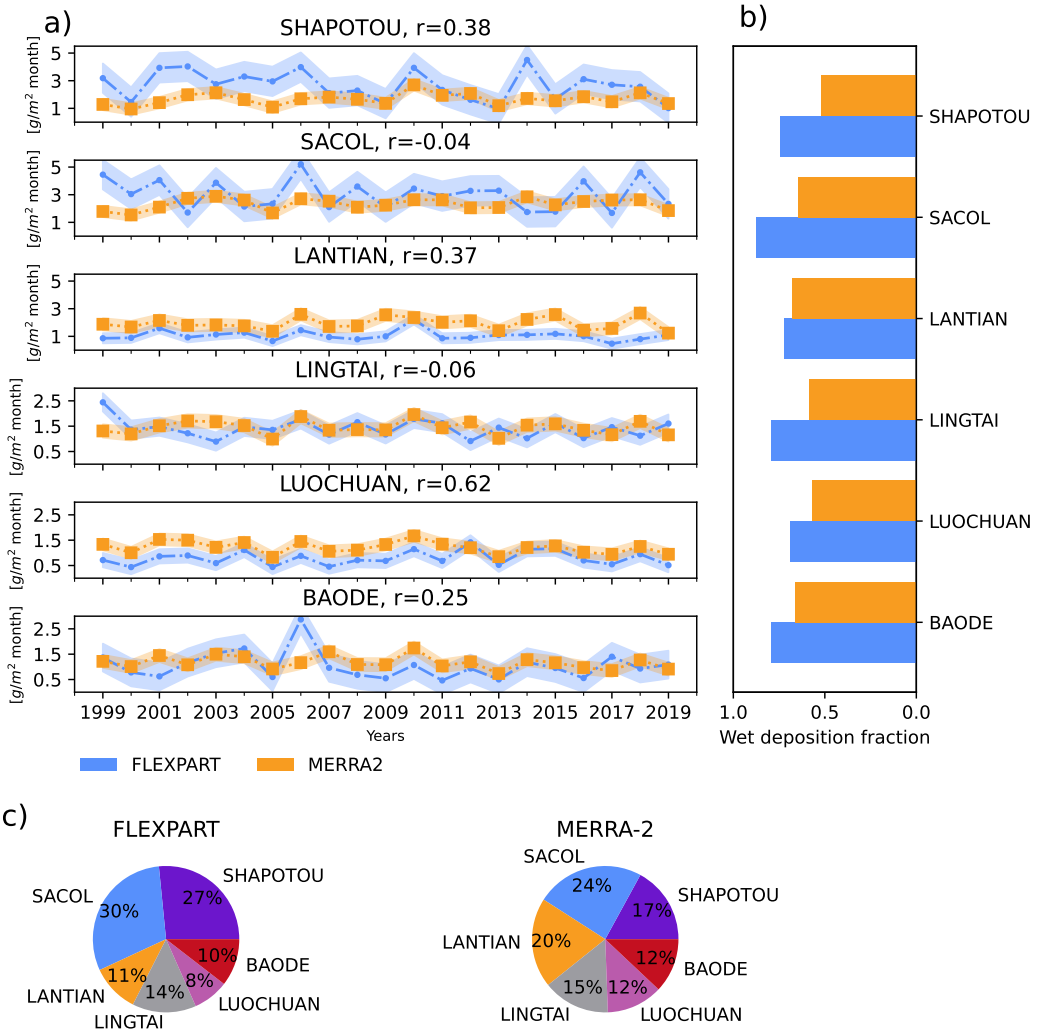


Figure 4. (a) Inter-annual variation of total spring deposition simulated by FLEXPART (blue) and MERRA-2 (orange) of the fine dust particle size bin (FLEXPART mean diameter $2.057 \mu\text{m}$, size bin 2 in MERRA-2, $1.0\text{-}1.8 \mu\text{m}$) for each of the sites at the CLP. The envelope indicates one standard deviation. (b) The ratio of wet deposition to total deposition at each receptor site. The blue bar is FLEXPART and orange bar is MERRA2. (c) Relative distribution of dust deposition between the receptor sites in FLEXPART and MERRA-2.

well for Luochuan, Lantian, and Shapotou, but FLEXPART and MERRA-2 are not correlated at SACOL and Lingtai. SACOL and Lingtai are located close to the mountains in a region with complex topography, which is not well resolved by typical model grids. Additionally, accurately representing precipitation in mountainous regions poses a significant challenge, and different reanalysis datasets may have substantial variation in their precipitation rates (J. Yao et al., 2020). Moreover, SACOL and Lingtai experience a high proportion of wet deposition, as shown in Figure 4b, making the differences in precipitation events between ERA5 and MERRA-2 a potential source of reduced correlation. There is a greater correlation in the dry deposition rate between MERRA-2 and FLEXPART for all sites (see Figure S1) than in wet deposition. In addition, the wet deposition has a larger interannual variation in FLEXPART compared to MERRA-2. Consequently, wet deposition amplify the differences between FLEXPART and MERRA-2 to total deposition. Finally, modeling dust (wet) deposition is an overarching problem in current dust models, with models showing large differences in the relative importance of wet to dry deposition (Zhao et al., 2022; Huneeus et al., 2011).

FLEXPART and MERRA-2 also show differences in the spatial distribution of dust deposition throughout the CLP (Figure 4c). MERRA-2 has a smaller spatial difference in dust deposition throughout the CLP, while in FLEXPART the two sites close to the source regions make up more than 50% of the combined deposition of our sites. Our set-up with backward trajectories limited to 10 days and the comparison of relatively larger sized particles in FLEXPART to smaller particles in MERRA-2 can both contribute to this model inconsistency, but it is also related to the longer lifetime in MERRA-2 compared to FLEXPART (Tang et al., 2023).

Although conducting a detailed investigation of the differences in the representation of the EADC in FLEXPART and MERRA-2 is outside the scope of this study. Still, our initial assessment has revealed that the interannual variation in dust emissions in FLEXDUST-EA shown in Figure 3 aligns well with that of MERRA-2, particularly for the important source regions in East Asia. However, total dust deposition over the CLP in FLEXPART is not consistent with MERRA-2 at all sites, mainly due to differences in the occurrence of wet deposition events. Evaluating the representation of dust deposition in both MERRA-2 and FLEXPART poses challenges due to the limited constraints available on dust deposition in East Asia and the rudimentary nature of dust deposition parameterization in models (X. Zhang et al., 2019).

3.2 Springtime dust transport to the Chinese Loess Plateau: wet versus dry deposition

Figure 5 shows the 20-year averaged spring source contribution maps for each site and both dust particle sizes. The source contribution is normalized by the mean contribution, enabling a relative comparison of the influence of different sources, independent of the deposition rate at the site. The pie chart represents the relative contribution of the source regions as defined in Figure 3 to the total deposition at the site.

Across all CLP locations, Figure 5 shows that the predominant source region that accounts for the majority of dust deposition is the deserts northwest of the CLP. Depending on the site, this source contributes between 48% and 78% of the fine dust and between 47% and 88% of the super-coarse dust. In particular, the source contribution of super-coarse dust in Figure 5 shows a higher contribution from nearby sources compared to fine dust. Fine dust shows a gradual transition from the primary dust sources to less influential ones as one moves away from the receptor location on the source contribution map. The relative source contributions

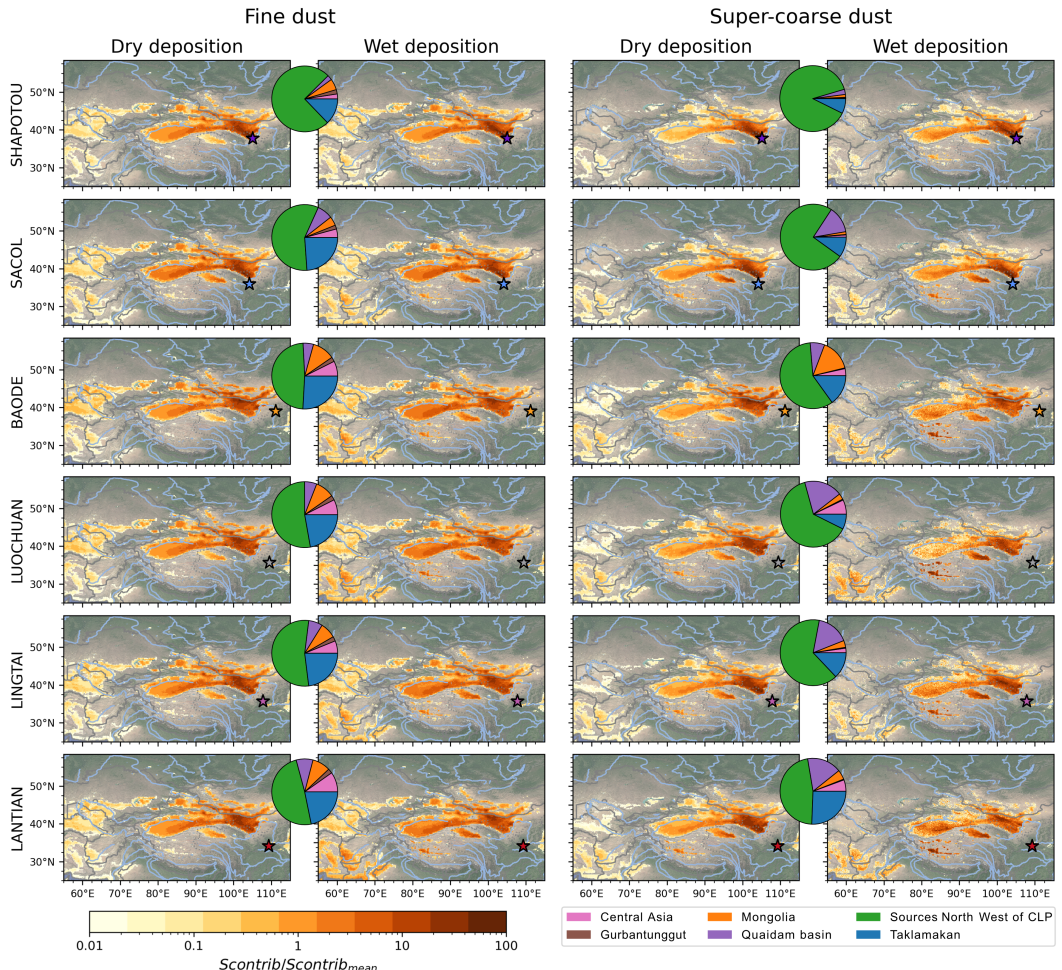


Figure 5. Averaged spring dust source contribution (1999–2019) of dry- and wet deposition scaled by the mean contribution. The pie chart shows the contribution from each of the source regions as defined in Figure 3.

385 of fine dust at our CLP locations shown in Figure 5 are consistently similar. For ex-
 386 ample, at Baode, Luochuan, Lingtai, and Lantian, the order of importance of the
 387 different source regions remains consistent: (1) Northwest deserts, (2) Taklamakan,
 388 (3) Mongolia, (4) Central Asia, (5) Qaidam Basin, and (6) Gurbantunggut desert.
 389 Even at SACOL and Shapotou, which have more distinct source contributions, the
 390 main difference lies in an increased contribution from the northwestern dust sources.

391 In contrast, the source composition of super-coarse dust displays more dis-
 392 tinct patterns at each location. For instance, super-coarse dust from Shapotou orig-
 393 inates primarily from the nearby desert to the northwest of the CLP, with only a
 394 minor contribution from Taklamakan. Baode experiences a substantial influx of
 395 super-coarse dust from Mongolia, a source nearly absent at other sites. Another no-
 396 table aspect of super-coarse dust is the trend of increasing influence of dust from
 397 the Qaidam Basin across the southeast transect of the CLP. Although the Qaidam
 398 Basin contributes modestly to emissions, it becomes the second most influential
 399 source at SACOL, Luochuan, Lingtai, and third at Lantian. Central Asia and the
 400 Gurbantunggut desert, although not primary sources of dust to the CLP, however,
 401 are not negligible at certain sites. For instance, Central Asia contributes to 6-7% of
 402 the super-coarse dust deposited at Lingtai and Lantian, emphasizing how even larger
 403 dust particles from distant dust emission regions can impact the CLP.

404 The difference between the dry and wet deposition source contribution is shown
 405 in Figure 5. The source contributions of wet and dry deposition of fine dust are
 406 mostly similar except for dry deposited dust being more influenced by the north-
 407 western sources, whereas wet deposition has a stronger influence from the more dis-
 408 tant sources. On the other hand, the source contribution of wet deposited super-
 409 coarse dust noticeably diverges from the sources of dry deposited dust. The wet
 410 deposition source contribution displays a more noisy pattern, indicating less fre-
 411 quent occurrences of wet deposition for super-coarse dust. The larger variability of
 412 the wet-deposited super-coarse dust translates into a more erratic spatial pattern
 413 in the wet deposition source contribution compared to the relatively robust pattern
 414 observed for dry deposition.

415 The source contribution maps presented in Figure 5 represent the cumulative
 416 effects of emissions, transport, and deposition. To pick out the general dust trans-
 417 port routes to the CLP, we take the centroid trajectory of all the particles released
 418 within each 3-hourly particle release and combine them into one dust transporting
 419 trajectory by calculating the center of mass of all the trajectories over the whole pe-
 420 riod weighted by the deposition rate modeled at the time of release. The dust trans-
 421 port trajectories for all sites and for dry and wet deposition are shown in Figure 6.
 422 In the case of fine dust, the trajectories demonstrate minimal variation between re-
 423 ceptor locations, consistent with relatively uniform source contribution maps across
 424 the different sites. Conversely, for super-coarse dust, the transport patterns of dry-
 425 deposited dust closely resemble those of dry-deposited fine dust, primarily exhib-
 426 iting a prevailing northwesterly transport (Figure 6 a, b). An exception is observed
 427 for SACOL, displaying a more westerly transport, in alignment with the substantial
 428 contribution from the Qaidam Basin. Wet deposition of super-coarse dust exhibits
 429 significant variability in transport trajectories between receptors, contributing to the
 430 site-dependent nature of super-coarse dust source contributions. A common trend
 431 across all sites is that wet-deposited dust is generally influenced by southerly air-
 432 masses, resulting in overall westerly transport. Given that the source of moisture
 433 originates from the south, this pattern is reasonable. Furthermore, the trajectories
 434 show an increase in altitude as they approach the receptor, indicating that wet-
 435 deposited dust typically experiences uplift due to convection initiated by the typical
 436 cold air advection observed during a dust event.

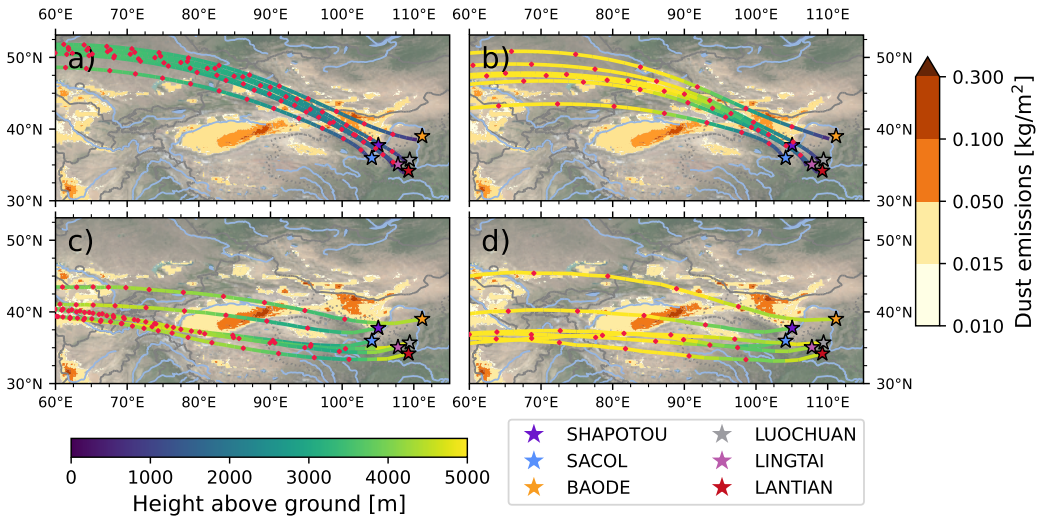


Figure 6. Weighted average centroid dust loading trajectories by the deposition rate at the receptor at the time of arrival. (a) and (b) are dry deposition dust loading trajectories for fine (mean diameter $2.057 \mu\text{m}$) and super-coarse dust (mean diameter $17.32 \mu\text{m}$) particles. (c) and (d) wet deposition dust loading trajectories for the fine and super-coarse dust respectively. The mean height is along the trajectory shown by the coloring and the red dots along the trajectories are equally spaced 12hours apart. The shading underneath show the mean dust emission rate.

Wind speed only changes the mass emitted for dust up to $20 \mu\text{m}$, but does not change the size distribution at emissions (Kok, 2011). Therefore, the variations in source contribution between fine and super-coarse dust primarily stem from differences in their lifetimes. In FLEXPART, we changed two parameters that control dust particle lifetime: the wet scavenging efficiency (assumed to be size-dependent) and the particle size that governs the dry deposition velocity. The impact of different gravitational settling can be seen from the difference in the source contribution between dry-deposited fine and super-coarse dust. To keep the super-coarse dust in the air sufficiently long enough to reach the CLP, either the wind speed has to be sufficiently strong such that the dust arrives before it falls out or the dust has to experience vertical lifting to counter the gravitational settling.

Topography has been proposed to increase vertical dust transport. Heisel et al. (2021) utilized high-resolution large-eddy simulations to demonstrate that gently sloping terrain can substantially amplify vertical dust transport. The source contribution maps of wet-deposited super-coarse dust showed a distinct band of higher contribution along the southern edge of the Taklamakan. Additionally, it is important to observe that this band of intensified source contribution is less prominent in the source contribution maps for dry deposition, suggesting that this phenomenon cannot be solely attributed to heightened emissions along the southern boundary. Moreover, similar to the Taklamakan, the Qaidam Basin, a source surrounded by sloping terrain, is also a substantial source of wet-deposited super-coarse dust. Hence, potentially suggesting that when super-coarse dust ascends to higher atmospheric levels, it becomes scavenged within the cloud and falls out with the precipitation. Particles of this size readily activate as Cloud Condensation Nuclei (CCN) and rapidly grow to raindrop size. Consequently, a substantial amount of coarse dust could potentially accelerate precipitation onset, mitigating the tendency

463 of continental air with high concentrations of CCN to produce numerous small cloud
 464 droplets (Posselt & Lohmann, 2008).

465 In summary, there are two prominent pathways for dust transport. The first
 466 pathway exhibits a prevailing northwesterly direction, gathering dust primarily from
 467 the northwestern desert regions. This pattern is strongly associated with the dry de-
 468 position of dust on the CLP. Conversely, the second dust transport pathway, linked
 469 to wet deposition, follows a more westerly trajectory. Along this route, topographi-
 470 cal features drive dust to higher atmospheric levels, where it is then scavenged within
 471 the clouds and subsequently washed out over the CLP.

472 3.3 Drivers of interannual variations in EADC

Table 2. Definition of the climatic indices used in the correlation analysis.

Indices	Definition	Reference
Arctic Oscillation (AO)	Leading EOF of the 1000hPa geopotential height anomalies poleward of 20°N	Thompson and Wallace (1998)
East Asian Winter Monsoon intensity index (EAWMI)	Difference in area averaged 300hPa zonal winds $U_{300}(27.5^{\circ}\text{--}37.5^{\circ}\text{N}, 110^{\circ}\text{--}170^{\circ}\text{E})$ - $U_{300}(50^{\circ}\text{--}60^{\circ}\text{N}, 80\text{--}140^{\circ}\text{E})$	Jhun and Lee (2004)
Monsoon Index (MO)	Difference in MSLP between two grid points (105°E, 52.5°N) near Irkutsk and (145°E, 43.75°N) near Nemuro.	Sakai and Kawamura (2009)
Siberian High intensity index (SHI)	Area averaged MSLP (40°-65°N, 80°-120°E)	Wang and Chen (2010)
East Asian Temperature Gradient (EATG)	Gradient in zonally averaged temperature between 30°- 120°E, and taken the averaged gradient between 40°and 50°N	J. Liu et al. (2020)

473 In the following, we utilize the FLEXPART simulations to examine the factors
 474 driving the interannual variations in the spring EADC over the past 21 years from
 475 1999 to 2019. We establish correlations between dust emission and deposition and
 476 various climatic variables representing different aspects of the East Asian circula-
 477 tion. The indices that we used, along with their definitions, are summarized in Table
 478 2. All indices are calculated from monthly ERA5 data for both winter (December-
 479 February) and spring (March-May). Decadal trends are removed from the time se-
 480 ries before calculating the correlations to avoid the influence of low-frequency cli-
 481 mate variations.

482 The correlations of the winter and spring circulation with spring dust emissions
 483 are shown in Figure 7b,c. Figure 7b shows that the circulation of the preceding win-
 484 ter has a significant impact on the frequency and intensity of dust storms in spring.
 485 Emissions from the northwestern deserts are anticorrelated with winter AO. As ev-
 486 ident in Figure 5 in the previous section, this is the most significant dust source for
 487 the CLP. Interestingly, winter AO does not significantly affect emissions from other
 488 source regions. Instead, Taklamakan emissions are negatively correlated with the
 489 winter monsoon and are most strongly correlated with the Siberian High Intensity
 490 Index (SHI), suggesting that the location and strength of the SH are important fac-
 491 tors that regulate dust emissions in the Taklamakan desert. Qaidam emissions have
 492 correlations similar to those of Taklamakan, albeit weaker. Emissions from Central
 493 Asia and Gurbantunggut are not strongly related to the winter circulation of East
 494 Asia. For the spring circulation shown in Figure 7c, dust emissions in Mongolia and



Figure 7. (a) Correlations between winter (December-January-February, DJF) and spring (March-April-May, MAM) circulation indices and modeled spring dry- and wet deposition of super-coarse dust, for the whole domain and contributions from individual source regions. (b-c) Correlation with FLEXDUST-EA dust emissions in the source regions and with winter and spring circulation respectively. The size of the circle indicate the strength of the correlation.

495 northwestern deserts are more strongly correlated with the magnitude of the East
 496 Asian Temperature Gradient (EATG), that is, a large negative temperature gradi-
 497 ent favors larger emissions. Taklamakan emissions do not show a significant corre-
 498 lation with any particular spring circulation index. Qaidam is similar again to Takla-
 499 makhan except that it is more positively correlated with AO. The intensity of the SH
 500 in spring is significantly anti-correlated with emissions from Central Asia and Gur-
 501 bantunggut.

502 Figure 7a shows the correlations between source contributions of super-coarse
 503 dust, delineated by contributions from each dust emission region to each site. Look-
 504 ing at the winter circulation, we observe significant negative correlations between the
 505 AO and dry deposition at Shapotou, SACOL, Baode, and Luochuan. Additionally,
 506 AO is negatively correlated with wet deposition at Lantian and SACOL. The corre-
 507 lations with AO are most pronounced for source contributions from Mongolia and
 508 the northwestern deserts, although they vary by site.

509 Interestingly, wet deposition at SACOL demonstrates significant correlations
 510 with all winter circulation indices, including AO and MO, both of which are linked
 511 to the EATG. Additionally, the SHI correlates with both AO and MO, even though
 512 AO and MO do not exhibit a significant correlation with each other (see Supplement
 513 Figure S3). Considering these insights, we infer that, for wet deposition at SACOL,
 514 the strength of EATG in winter plays a critical role in creating favorable conditions
 515 for wet deposition in spring, mainly sourced from the northwestern deserts. How-
 516 ever, for dry deposition at SACOL, AO is the only significantly correlated index,
 517 aligning with AO's correlation with emissions from the northwestern sources, the
 518 primary dust source for SACOL.

519 The strength of the EAWM is correlated with dust from Qaidam and Gurban-
 520 tunggut to the SACOL site. The spring EAWM circulation features are correlated
 521 with an increased contribution from the Gurbantunggut desert to Lantian, Lingtai,
 522 and Luochuan. The deposition of Central Asian dust at the sites is generally not
 523 correlated with any of the circulation indicators, except at Baode site, which shows a
 524 significant negative correlation between the contribution of dry deposited dust from
 525 Central Asia and the SHI, where the SH can act as a barrier for long-range dust
 526 transport.

527 The correlations presented above are for the super-coarse dust size bin. Fine
 528 dust correlations are provided in the Supplement (Figure S4). The correlations be-
 529 tween the winter AO circulation and spring deposition remain consistent across fine
 530 and super-coarse dust. However, in terms of spring circulation, the two particle sizes
 531 are less consistent. Dry-deposited fine dust displays notably higher correlations with
 532 EATG and EAWMI, especially for dust transport from Taklamakan compared to
 533 super-coarse dust. For the north western deserts fine and super-coarse dust exhibit
 534 similar correlations with EATG. The correlations between circulation patterns and
 535 wet deposition for fine dust are highly variable and strongly dependent on the site,
 536 and this does not change from what is shown in Figure 5. This underscores that wet
 537 deposition is the result of an intricate dynamic between the source, receptor, and
 538 circulation modes.

539 To interpret the relationship between atmospheric circulation patterns and
 540 dust deposition over the CLP, as revealed in the previous correlation analysis shown
 541 in 7, we performed a composite analysis of years with weak and strong deposition
 542 at sites, to identify site-dependent circulations features that typically cause an in-
 543 crease in dust deposition. Figure 8 shows the composite differences of 850hPa winds
 544 and mean sea level pressure (MSLP), hatched areas show the regions where the dif-
 545 ferences between the strong and weak dust deposition years are significant. In the
 546 case of dry deposition of super-coarse dust, all sites manifest AO-like composite dif-

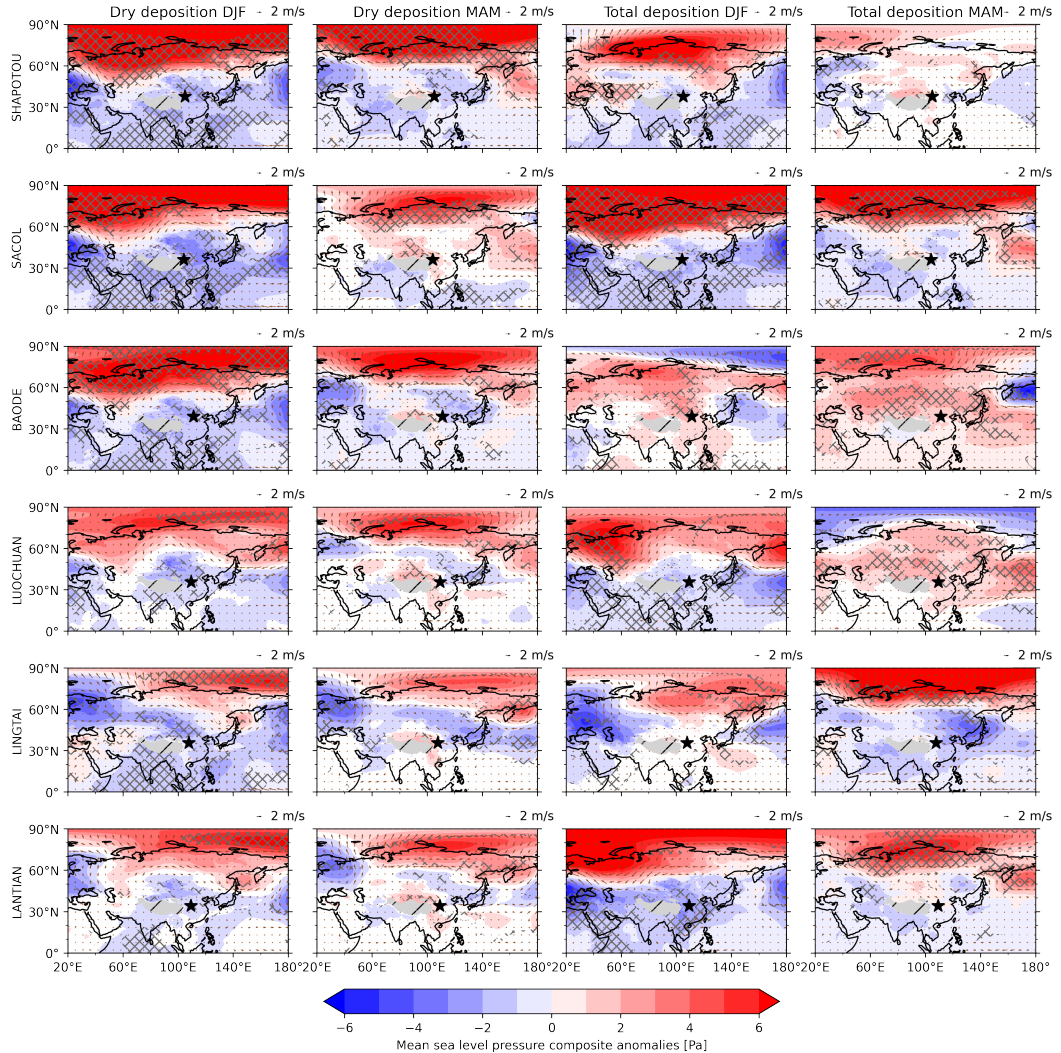


Figure 8. Composite difference of mean sea level pressure and 850hPa wind strong minus weak deposition years for super coarse dust for both winter (December-January-February, DJF) and spring (March-April-May, MAM) for all the locations. The left half shows composite difference based on dry deposition rate, while the right half is the composite difference based on total deposition rate. The hatched area indicates where the anomalies are significant ($p < 0.05$)

547 differences during the winter preceding a strong deposition year. These anomalies show
 548 characteristic positive MSLP anomalies over the Arctic, typical of negative AO-like
 549 conditions (Thompson & Wallace, 1998; He et al., 2017). This AO-like pattern ex-
 550 tends into the spring for most sites. However, for total deposition at Shapotou and
 551 Luochuan, the AO pattern is masked by other influences, as wet deposition is more
 552 event-dependent and less influenced by the overarching circulation state. A longer
 553 time series of simulations would be able to better distinguish the more random fluc-
 554 tuations due to wet deposition from the impact of large-scale circulation.

555 Figure 9 shows the composite anomalies of the geopotential height and winds
 556 at 500hPa for super-coarse dust. During the winter preceding a strong deposition
 557 year, it indicates an area of reduced geopotential height that for Lantian, Lingtai,
 558 Luochuan and Baode is located to the north west of the site, while for Shapotou
 559 and SACOL negative geopotential height anomaly is located more to the north east.
 560 This suggests that increases in dust deposition as a result of dry deposition at these
 561 sites are closely associated with the location of this geopotential height anomaly and
 562 the corresponding changes in the wind patterns.

563 During the negative phase of AO, there is usually an increase in the frequency
 564 and intensity of cold air outbreaks (COAB) in East Asia (He et al., 2017; Yang et
 565 al., 2020). H. Liu et al. (2018) conducted a detailed analysis investigating the rela-
 566 tionship between spring dust emissions and the preceding winter AO using MERRA-
 567 2 reanalysis. Using regression analysis, they revealed a correspondence between win-
 568 ter 500 hPa geopotential height and the leading empirical orthogonal function of
 569 spring dust emissions, similar to the composite anomalies we found shown in Figure
 570 9. H. Liu et al. (2018) suggested that a negative AO results in anomalous cold con-
 571 ditions in central Siberia, which persist into the ensuing spring, amplified by snow-
 572 albedo and cloud feedbacks. The resultant colder temperatures in the inner regions
 573 of East Asia create a more negative temperature gradient in the region, intensify-
 574 ing the East Asian Trough (EAT). This in turn creates a favorable environment for
 575 dust emissions. Their explanation of how winter AO influences spring surface tem-
 576 perature aligns with our correlation analysis, where a negative AO corresponds to a
 577 more pronounced temperature gradient over East Asia, elevating dust transport to
 578 the CLP from the northwestern sources.

579 3.4 Implications for interpreting Chinese Loess Plateau dust records

580 Our results reveal a clear link between the depositional mechanism and the
 581 dust-emitting regions. This observation may have major implications on how we in-
 582 terpret the provenance of the CLP dust records (Quaternary loess and Neogene red
 583 clay) also on geological time scales. The CLP dust provenance studies often con-
 584 sider changes in emission and transport mechanisms, but commonly overlook the fi-
 585 nal step of the EADC, the deposition. Our results on the deposition of both fine and
 586 super-coarse particles indicate that wet deposition contains more dust from west-
 587 ern emission areas than dry deposition (Figure 6), suggesting the shift in CLP dust
 588 provenance may not only be related to changes in dust transport pathways but also
 589 the deposition mode. The CLP dust records are associated with coarser grain sizes
 590 during glacials compared to interglacials. These differences have been explained by
 591 higher dust influx and reduced soil development coupled with stronger wind speeds
 592 during glacial periods (Maher, 2016; Kohfeld & Harrison, 2003). However, our re-
 593 sults imply that increased wet deposition of fine/clay-sized dust during the wetter
 594 interglacials could provide an additional explanation for the observed grain-size dif-
 595 ferences between glacials and interglacials. Similarly, the finer grain size of late Neo-
 596 gene red clay deposits compared to Quaternary loess may be associated with an in-
 597 crease in the wet deposition of finer particles during intensified EASM conditions
 598 (Ren et al., 2020; Z. L. Ding et al., 1999).

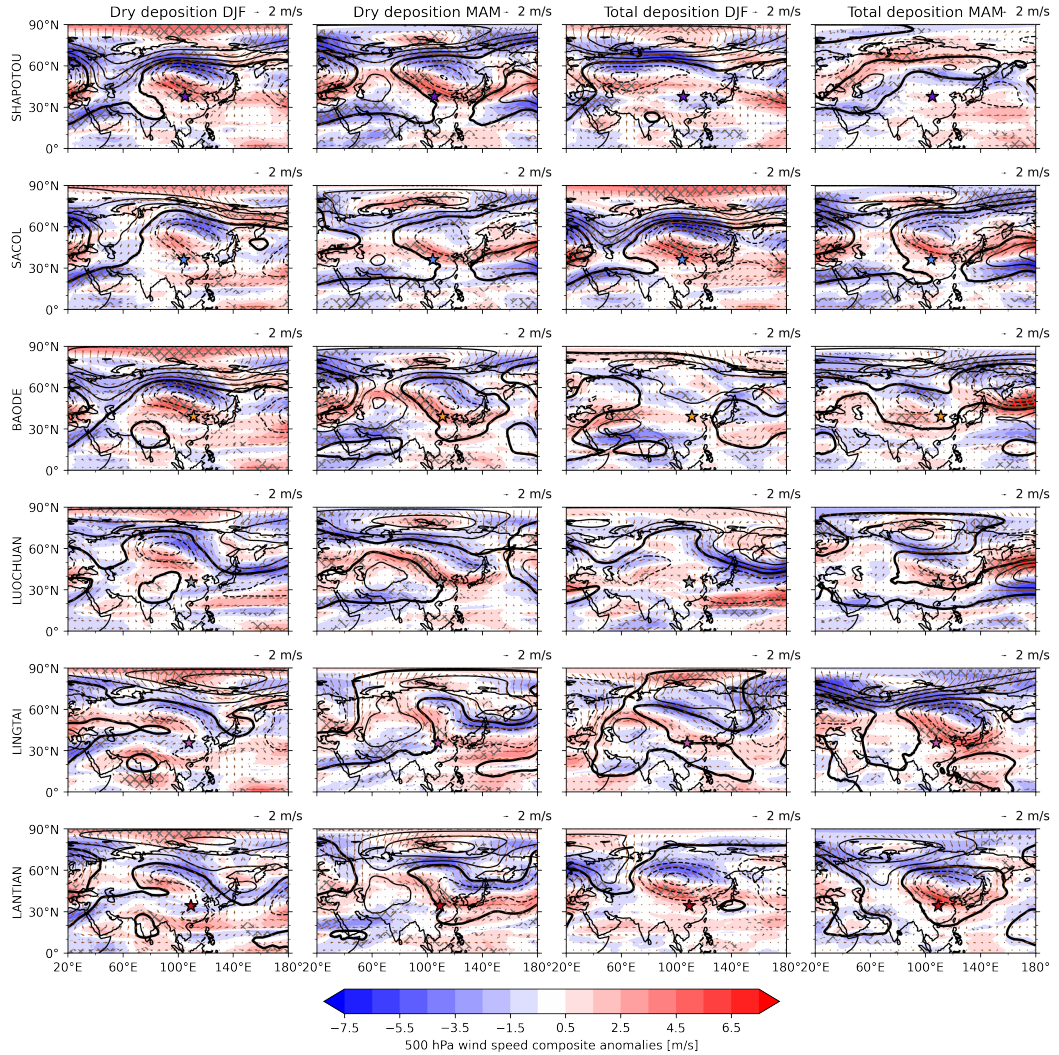


Figure 9. Circulation composite anomalies of 500hPa wind strength (colored, unit m/s), wind direction (vectors, unit m/s) and geopotential height (contours, unit dam, distance between contours 2 dam, solid contour are positive anomalies while dotted contours are negative anomalies) for winter (December-January-February, DJF) and spring (March-April-May, MAM) of strong - weak dry and total deposition years. The hatched area indicates where the anomalies are significant ($p < 0.05$)

The results of our model, which covers the full dust cycle (i.e., emission, transport, and deposition), may also have important implications on the observed spatial differences in source contribution across the CLP. Previous single-grain provenance studies (targeting silt-sized particles) have documented Neogene and Quaternary dust source differences between the northeastern (e.g., Baode site) and the southwestern (e.g., Lantian) CLP (Shang et al., 2016; H. Zhang et al., 2021; W. Peng et al., 2023; Bird et al., 2015). These observations were supported by backward trajectory modeling showing more dominant atmospheric transport pathways from the Taklamakan desert and Northern Tibetan Plateau to the southwestern CLP than to the northeastern CLP (Shang et al., 2016). The results of our model, taking into account the full EADC, further corroborate these conclusions (Figure 5). In addition, spatial differences in dust provenance have been found to be particularly prominent in coarse dust particles and wet deposited dust (Figure 5). This offers a plausible eolian mechanism for explaining the spatial provenance contrast of the red clay and loess deposits, and its temporal variations, in addition to the well-established hypothesis emphasizing the importance of large fluvial systems (namely the Yellow River) in providing dust particles closer to the CLP, and therefore in creating the observed spatial provenance gradient (Stevens et al., 2013; Bird et al., 2015; Nie et al., 2015; W. Peng et al., 2023; H. Zhang et al., 2021 ;Sun et al., 2022). For instance, W. Peng et al. (2023) found an increase in Pliocene spatial provenance contrast in the Red Clay, and argued that this was partly caused by the intensified Pliocene EASM. This argument is well in line with our results, since the intensified EASM can enhance the wet deposition flux over the CLP. Therefore, an increase in wet deposition can act to amplify the spatial provenance differences created primarily by the fluvial input of material.

Our modeling results with super-coarse/silt-sized dust particles indicate that even large dust particles deposited on the CLP may be sourced from distant dust-emitting sources (e.g., Taklamakan) although they are not the dominant contributor to the deposition on the CLP. Larger dust particles (super-coarse or larger) deposited far from the dust emission region have also been reported in recent observational studies (Van Der Does et al., 2018; Ryder et al., 2018; A. A. Adebiyi & Kok, 2020). The fact that we also find reason to believe that super-coarse dust deposited over the CLP can be from the distant dust-emitting regions provides additional support to the validity of the single-grain provenance proxy studies using mainly the large mineral particles in detecting the source origin of emitted dust. Strengthening claims and insights on loess formation mechanisms and climatic implications made based on the coarse dust fractions in the loess deposits. We note that spherical particles are assumed in our model simulations, thus might be considered a lower bound of the long-distance transport of super-coarse dust to the CLP. Further modeling studies using a-spherical particles with lower settling velocities and potentially longer transport distance than spherical particles may help to better understand the long-distance transport of large dust particles.

The interannual variation of the spring dust deposition rate over the CLP has been found to be more closely associated with AO than with the strength of the EAWM in both winter and spring (Figure 7 and S4). This is distinct from the common understanding within the paleoclimate communities which emphasizes the importance of EAWM in regulating the dust cycle over the CLP (e.g. An et al., 2014). However, consistent with studies of the present-day interannual variation of the EADC, which generally support the strong control of AO instead of EAWM on the variation of EADC (Mao et al., 2011; H. Liu et al., 2018), with the negative AO being favorable for stronger dust storms in East Asia. Although the results are based on the annual time scale, they may have strong implications for understanding long-term changes in the EADC and the interpretation of the red clay and loess record, especially when it is difficult to use the strength of EAWM to explain the dust records

and its variations. For instance, provenance research on the dust records deposited during the warmhouse Eocene indicates the absence (or significantly weaker) SH coupled with possible long-term negative phase of AO-like conditions (Bohm et al. 2023X, in revision). Moreover, it has been noticed that the cyclicity of the oxygen isotopes of speleothem records over East Asia, an indicator of East Asian summer monsoon, is dominated by precession cycle (20 ka) on orbital time scale, which is in contrast to the loess records, which reveal a dominance of the glacial-interglacial cycle (100 ka) (Cheng et al., 2021). The larger influence of AO-like conditions (over EAWM) on the variation of dust deposition over the CLP during the glacial-interglacial cycle, may offer a plausible explanation of the "apparent" discrepancy between loess and speleothem records from East Asia. This explanation is consistent with the fact that high-latitude forcing is the dominant influence on Loess records (Stevens et al., 2018). However, on the basis of this work, it is not possible to conclude whether this is generally the case because the climatic conditions during the glacial stages are very different from those of today. Although, this could be answered by driving this modeling setup using data from paleoclimate simulations in the future.

4 Conclusion

To our knowledge, this is the first modeling study to provide a detailed picture of how proximate and distant dust emission areas contribute to dust accumulation on the CLP. We provide evidence for the importance of considering wet deposition when interpreting the loess records, showing that wet-deposited dust differs in both the typical transport trajectory and the source of the emitted dust. Even super-coarse dust could be wet deposited at the CLP where sloping topography upwind of dust emission area can act to increase the vertical dust transport substantially, making it possible for even large dust particles to be scavenged inside clouds. This could be an important mechanism for bringing potentially non-negligible amounts on of coarse dust particles from more distant sources like the Taklamakan desert and Quaidam basin. Dry-deposited dust is mainly sourced from the nearby dust-emitting areas to the north-west of the CLP, this transport pathway is favorable under negative AO-like conditions. That the AO is an important driver of the EADC is in line with our understanding of the EADC under present day climate conditions (H. Liu et al., 2018; Mao et al., 2011; D.-Y. Gong et al., 2006). This study provides a direct link between AO and dust accumulation on the CLP. Our link between AO and dust accumulation on the CLP was established based on current climate conditions, which were different in the past, but it does warrant a stronger emphasis on high-latitude forcings when explaining the variability in dust accumulation rate of the loess record rather than the common partitioning of enhanced summer monsoon or winter monsoon conditions, as also suggested by Roe (2009).

FLEXPART has also been shown to be a very useful tool for understanding the dust cycle, as it can pinpoint the exact dust source contribution of a receptor site. The FLEXPART ES is independent of the dust emission inventory, so FLEXPART can be used to easily test the effect and impact of different emission schemes and hypothesis of changes in dust emission regions in the past. A promising future application of this setup would be to combine FLEXPART and state-of-the-art paleoclimate model reconstructions to give insight into how environmental changes have influenced the source region and dust transport mechanism at the CLP. This would be invaluable information to further aid in interpretation of the CLP provenance proxies and help to understand how the EADC might change in the future.

702 Acronyms

- 703 CAOB** Cold air outbreaks
704 EAWM East Asian Winter Monsoon
705 CLP Chinese Loess Plateau
706 AO Arctic Oscillation
707 LPDM Lagrangian particle dispersion model
708 MAR Mass accumulation rate
709 EOF Empirical orthogonal functions
710 MSLP Mean sea level pressure
711 DJF December January February
712 MAM March April May
713 EADC East Asian dust cycle
714 ES Emission sensitivity
715 SHI Siberian High Intensity index
716 EATG East Asian Tempereature Gradient
717 MO Monsoon index

718 Acknowledgments

This work was supported by the Research Council of Finland (grant no 316799).
The simulations were performed on resources provided by Sigma2 - the National Infrastructure for High Performance Computing and Data Storage in Norway, project no. nn2806k. The MERRA-2 data used in this study have been provided by the Global Modeling and Assimilation Office (GMAO) at NASA Goddard Space Flight Center and are available from NASA GES DISC (<https://disc.gsfc.nasa.gov/datasets?project=MERRA-2> last access October 2021). ERA5 data used in this study were downloaded using the Copernicus Climate Change Service (C3S) Climate Data Store. Neither the European Commission nor ECMWF is responsible for any use that may be made of the information it contains.

The FLEXDUST-EA source code is available at https://github.com/huitang-earth/FLEXDUST/tree/FES2022_Tangetal_updated_KOK14, and the FLEXPART codes are available at <https://github.com/Ovewh/flextpart/tree/release-10>. The workflows for setting up the FLEXPART simulations are available on github: <https://github.com/MasterOnDust/FLEXPART-script/releases/tag/>) The workflow for post-processing the raw simulation output and combining the FLEXDUST emission inventory with FLEXPART ES is available on GitHub (https://github.com/MasterOnDust/FP_preprosses_workflow/tree/AGU-Haugvaldstad-et-al-2023). The workflow to generate the figures shown in this manuscript is available in the following GitHub repository:https://github.com/MasterOnDust/AGU_JGR_CLP_SOURCE_WORKFLOW/tree/AGU-Haugvaldstad-et-al-2023 . The data files required to generate the figures shown in the manuscript are available from Zenodo Haugvaldstad et al. (2023) <https://doi.org/10.5281/zenodo.10114436>. The full 3hourly FLEXPART source contribution, emission sensitivity and FLEXDUST dust emission inventory are archived on the Norwegian Research Data Archive; see (DOI: <https://doi.org/10.11582/2023.00134>, <https://doi.org/10.11582/2023.00135>), Haugvaldstad (2023a, 2023b).

746 References

- Adebiyi, A., Kok, J. F., Murray, B. J., Ryder, C. L., Stuut, J.-B. W., Kahn, R. A., ... Meng, J. (2023). A review of coarse mineral dust in the Earth system.

- 749 *Aeolian Research*, 60. doi: 10.1016/j.aeolia.2022.100849
- 750 Adebiyi, A. A., & Kok, J. F. (2020). Climate models miss most of the coarse dust in
 751 the atmosphere. *Science Advances*, 6(15), eaaz9507. Retrieved from <https://www.science.org/doi/abs/10.1126/sciadv.aaz9507> doi: 10.1126/sciadv.aaz9507
- 752 An, Z., Sun, Y., Chang, H., Zhang, P., Liu, X., Cai, Y., ... Jin, Z. (2014). Late
 753 Cenozoic Climate Change in Monsoon-Arid Asia and Global Changes. In
 754 Z. An (Ed.), *Late Cenozoic Climate Change in Asia: Loess, Monsoon and*
 755 *Monsoon-arid Environment Evolution* (pp. 491–581). Dordrecht: Springer
 756 Netherlands. Retrieved 2021-08-12, from https://doi.org/10.1007/978-94-007-7817-7_6 doi: 10.1007/978-94-007-7817-7_6
- 757 Bird, A., Stevens, T., Rittner, M., Vermeesch, P., Carter, A., Andò, S., ... others
 758 (2015). Quaternary dust source variation across the chinese loess plateau.
 759 *Palaeogeography, Palaeoclimatology, Palaeoecology*, 435, 254–264. doi: <https://doi.org/10.1016/j.palaeo.2015.06.024>
- 760 Bohm, K., Kaakinen, A., Stevens, T., Lahaye, Y., O'Brien, H., Tang, H., ... Lu, H.
 761 (2023). Neogene global climate change and East Asian dust sources: Combined
 762 rutile geochemistry and zircon U-Pb analysis from the northern Chinese Loess
 763 Plateau. *Global and Planetary Change*, 221. doi: 10.1016/j.gloplacha.2023
 764 .104049
- 765 Börker, J., Hartmann, J., Amann, T., & Romero-Mujalli, G. (2018). Global uncon-
 766 solidated sediments map database v1. 0 (shapefile and gridded to 0.5 spatial
 767 resolution). *Bremerhaven: PANGAEA*, 10.
- 768 Cheng, H., Zhang, H., Cai, Y., Shi, Z., Yi, L., Deng, C., ... Perez-Mejías, C. (2021,
 769 April). Orbital-scale Asian summer monsoon variations: Paradox and ex-
 770 ploration. *Science China Earth Sciences*, 64(4), 529–544. Retrieved 2023-
 771 10-18, from <https://doi.org/10.1007/s11430-020-9720-y> doi: 10.1007/
 772 s11430-020-9720-y
- 773 Choi, Y., Kanaya, Y., Takigawa, M., Zhu, C., Park, S.-M., Matsuki, A., ... Pisso,
 774 I. (2020, November). Investigation of the wet removal rate of black car-
 775 bon in East Asia: validation of a below- and in-cloud wet removal scheme in
 776 FLEXible PARTicle (FLEXPART) model v10.4. *Atmospheric Chemistry*
 777 and Physics, 20(21), 13655–13670. Retrieved 2021-03-18, from <https://acp.copernicus.org/articles/20/13655/2020/> (Publisher: Copernicus
 778 GmbH) doi: 10.5194/acp-20-13655-2020
- 779 de Sousa, L. M., Poggio, L., Batjes, N. H., Heuvelink, G. B. M., Kempen, B.,
 780 Riberio, E., & Rossiter, D. (2020). Soilgrids 2.0: producing quality-assessed
 781 soil information for the globe. *SOIL Discussions*, 2020, 1–37. Retrieved
 782 from <https://soil.copernicus.org/preprints/soil-2020-65/> doi:
 783 10.5194/soil-2020-65
- 784 Ding, Z., Sun, J., Rutter, N. W., Rokosh, D., & Liu, T. (1999). Changes in Sand
 785 Content of Loess Deposits along a North–South Transect of the Chinese Loess
 786 Plateau and the Implications for Desert Variations. *Quaternary Research*,
 787 52(1). doi: 10.1006/qres.1999.2045
- 788 Ding, Z. L., Xiong, S. F., Sun, J. M., Yang, S. L., Gu, Z. Y., & Liu, T. S. (1999, Au-
 789 gust). Pedostratigraphy and paleomagnetism of a ~7.0 Ma eolian loess-red
 790 clay sequence at Lingtai, Loess Plateau, north-central China and the im-
 791 plications for paleomonsoon evolution. *Palaeogeography, Palaeoclimatol-*
 792 *ogy, Palaeoecology*, 152(1), 49–66. Retrieved 2023-10-13, from <https://www.sciencedirect.com/science/article/pii/S0031018299000346> doi:
 793 10.1016/S0031-0182(99)00034-6
- 794 Dubovik, O., Holben, B., Eck, T. F., Smirnov, A., Kaufman, Y. J., King, M. D.,
 795 ... Slutsker, I. (2002, February). Variability of Absorption and Optical
 796 Properties of Key Aerosol Types Observed in Worldwide Locations. *Journal*
 797 *of the Atmospheric Sciences*, 59(3), 590–608. Retrieved 2023-10-16, from
 798
 799
 800
 801
 802
 803

- 804 https://journals.ametsoc.org/view/journals/atsc/59/3/1520-0469
805 _2002_059_0590_voaaop_2.0.co_2.xml (Publisher: American Meteorological Society Section: Journal of the Atmospheric Sciences) doi: 10.1175/1520-0469(2002)059<0590:VOAAOP>2.0.CO;2

806 Eckhardt, S., Cassiani, M., Evangelou, N., Sollum, E., Pisso, I., & Stohl, A. (2017).
807 Source-receptor matrix calculation for deposited mass with the lagrangian particle dispersion model flexpart v10.2 in backward mode. *Geoscientific Model Development*, 10(12), 4605–4618. Retrieved from <https://gmd.copernicus.org/articles/10/4605/2017/> doi: 10.5194/gmd-10-4605-2017

808 Eckhardt, S., Prata, A., Seibert, P., Stebel, K., & Stohl, A. (2008). Estimation of
809 the vertical profile of sulfur dioxide injection into the atmosphere by a volcanic
810 eruption using satellite column measurements and inverse transport modeling.
811 *Atmospheric Chemistry and Physics*, 8(14), 3881–3897.

812 Gelaro, R., McCarty, W., Su?rez, M. J., Todling, R., Molod, A., Takacs, L., ...
813 Zhao, B. (2017). The modern-era retrospective analysis for research and applications, version 2 (merra-2). *Journal of Climate*, 30(14), 5419 - 5454. Retrieved from <https://journals.ametsoc.org/view/journals/clim/30/14/jcli-d-16-0758.1.xml> doi: 10.1175/JCLI-D-16-0758.1

814 Gong, D.-Y., Mao, R., & Fan, Y.-D. (2006). East asian dust storm and weather disturbance: possible links to the arctic oscillation. *International Journal of Climatology: A Journal of the Royal Meteorological Society*, 26(10), 1379–1396.

815 Gong, S. L., Zhang, X. Y., Zhao, T. L., Zhang, X. B., Barrie, L. A., McKendry, I. G., & Zhao, C. S. (2006). A simulated climatology of asian dust aerosol and its trans-pacific transport. part ii: Interannual variability and climate connections. *Journal of Climate*, 19(1), 104 - 122. Retrieved from <https://journals.ametsoc.org/view/journals/clim/19/1/jcli3606.1.xml> doi: <https://doi.org/10.1175/JCLI3606.1>

816 Groot Zwaftink, C. D., Aas, W., Eckhardt, S., Evangelou, N., Hamer, P., Johnsrud, M., ... Yttri, K. E. (2022, March). What caused a record high PM₁₀ episode in northern Europe in October 2020? *Atmospheric Chemistry and Physics*, 22(6), 3789–3810. Retrieved 2023-10-30, from <https://acp.copernicus.org/articles/22/3789/2022/> (Publisher: Copernicus GmbH) doi: 10.5194/acp-22-3789-2022

817 Groot Zwaftink, C. D., Arnalds, O., Dagsson-Waldhauserova, P., Eckhardt, S., Prospero, J. M., & Stohl, A. (2017). Temporal and spatial variability of ice-landic dust emissions and atmospheric transport. *Atmospheric Chemistry and Physics*, 17(17), 10865–10878. Retrieved from <https://acp.copernicus.org/articles/17/10865/2017/> doi: 10.5194/acp-17-10865-2017

818 Groot Zwaftink, C. D., Grythe, H., Skov, H., & Stohl, A. (2016). Substantial contribution of northern high-latitude sources to mineral dust in the arctic. *Journal of Geophysical Research: Atmospheres*, 121(22), 13,678-13,697. Retrieved from <https://agupubs.onlinelibrary.wiley.com/doi/abs/10.1002/2016JD025482> doi: 10.1002/2016JD025482

819 Grythe, H., Kristiansen, N. I., Groot Zwaftink, C. D., Eckhardt, S., Ström, J., Tunved, P., ... Stohl, A. (2017). A new aerosol wet removal scheme for the lagrangian particle model flexpart v10. *Geoscientific Model Development*, 10(4), 1447–1466. Retrieved from <https://gmd.copernicus.org/articles/10/1447/2017/> doi: 10.5194/gmd-10-1447-2017

820 Guo, Z. T., Ruddiman, W. F., Hao, Q. Z., Wu, H. B., Qiao, Y. S., Zhu, R. X., ... Llu, T. S. (2002, 3). Onset of asian desertification by 22 myr ago inferred from loess deposits in china. *Nature* 2002 416:6877, 416, 159-163. Retrieved from <https://www.nature.com/articles/416159a> doi: 10.1038/416159a

821 Haugvaldstad, O. W. (2023a). *FLEXDUST simulated spring dust emissions of Asian dust from 1999-2019*. Archive2014. Retrieved 2023-11-20, from <https://archive.sigma2.no/pages/public/datasetDetail.jsp?id=10.11582/>

- 859 2023.00134 doi: 10.11582/2023.00134
- 860 Haugvaldstad, O. W. (2023b). *FLEXPART modelled source contributions of emitted*
 861 *dust over the Chinese Loess Plateau 1999-2019*. Archive2014. Retrieved 2023-
 862 11-20, from <https://archive.sigma2.no/pages/public/datasetDetail.jsf?id=10.11582/2023.00135> doi: 10.11582/2023.00135
- 863 Haugvaldstad, O. W., Tang, H., Kaakinen, A., Grythe, H., Groot Zwaftink, C., &
 864 Stordal, F. (2023, November). *Dataset Associated with Haugvaldstad et al*
 865 *2023 Spatial source contribution and interannual variation in deposition of dust*
 866 *aerosols over the Chinese Loess Plateau*. Zenodo. Retrieved from <https://doi.org/10.5281/zenodo.10114436> doi: 10.5281/zenodo.10114436
- 867 He, S., Gao, Y., Li, F., Wang, H., & He, Y. (2017). Impact of arctic oscillation
 868 on the east asian climate: A review. *Earth-Science Reviews*, 164, 48-62.
 869 Retrieved from <https://www.sciencedirect.com/science/article/pii/S0012825216303944> doi: <https://doi.org/10.1016/j.earscirev.2016.10.014>
- 870 Heisel, M., Chen, B., Kok, J. F., & Chamecki, M. (2021). Gentle Topography Increases Vertical Transport of Coarse Dust by Orders of Magnitude. *Journal of Geophysical Research: Atmospheres*, 126(14), e2021JD034564. Retrieved 2023-10-03, from <https://onlinelibrary.wiley.com/doi/abs/10.1029/2021JD034564> (_eprint: <https://agupubs.onlinelibrary.wiley.com/doi/pdf/10.1029/2021JD034564>) doi: 10.1029/2021JD034564
- 871 Hersbach, H., Bell, B., Berrisford, P., Hirahara, S., Horányi, A., Muñoz-Sabater, J.,
 872 ... Thépaut, J.-N. (2020). The ERA5 global reanalysis. *Quarterly Journal of*
 873 *the Royal Meteorological Society*, 146(730), 1999–2049. Retrieved 2021-01-25,
 874 from <http://rmet.s.onlinelibrary.wiley.com/doi/abs/10.1002/qj.3803>
 875 doi: <https://doi.org/10.1002/qj.3803>
- 876 Hooper, J., & Marx, S. (2018, October). A global doubling of dust emissions during
 877 the Anthropocene? *Global and Planetary Change*, 169, 70–91. Retrieved
 878 2021-12-06, from <https://www.sciencedirect.com/science/article/pii/S09218118300481> doi: 10.1016/j.gloplacha.2018.07.003
- 879 Huang, Y., Kok, J. F., Kandler, K., Lindqvist, H., Nousiainen, T., Sakai, T.,
 880 ... Jokinen, O. (2020). Climate Models and Remote Sensing Retrievals Neglect Substantial Desert Dust Asphericity. *Geophysical Research Letters*, 47(6), e2019GL086592. Retrieved 2023-07-18, from <https://onlinelibrary.wiley.com/doi/abs/10.1029/2019GL086592> (_eprint: <https://agupubs.onlinelibrary.wiley.com/doi/pdf/10.1029/2019GL086592>) doi: 10.1029/2019GL086592
- 881 Huneeus, N., Schulz, M., Balkanski, Y., Griesfeller, J., Prospero, J., Kinne, S., ...
 882 Zender, C. S. (2011, August). Global dust model intercomparison in AeroCom phase I. *Atmospheric Chemistry and Physics*, 11(15), 7781–7816. Retrieved
 883 2023-01-03, from <https://acp.copernicus.org/articles/11/7781/2011/acp-11-7781-2011.html> (Publisher: Copernicus GmbH) doi: 10.5194/acp-11-7781-2011
- 884 Jhun, J.-G., & Lee, E.-J. (2004). A new east asian winter monsoon index and associated characteristics of the winter monsoon. *Journal of Climate*, 17(4), 711–726.
- 885 Kohfeld, K., & Harrison, S. (2003). Glacial-interglacial changes in dust deposition on the chinese loess plateau. *Quaternary Science Reviews*, 22(18), 1859-1878. Retrieved from <https://www.sciencedirect.com/science/article/pii/S0277379103001665> (Loess and the Dust Indicators and Records of Terrestrial and Marine Palaeoenvironments (DIRTMAP) database) doi: [https://doi.org/10.1016/S0277-3791\(03\)00166-5](https://doi.org/10.1016/S0277-3791(03)00166-5)
- 886 Kok, J. F. (2011, January). A scaling theory for the size distribution of emitted dust aerosols suggests climate models underestimate the size of the global dust cycle. *Proceedings of the National Academy of Sciences*, 108(3), 1016–1021.

- 914 Retrieved 2021-03-18, from <https://www.pnas.org/content/108/3/1016>
 915 (ISBN: 9781014798107 Publisher: National Academy of Sciences Section:
 916 Physical Sciences) doi: 10.1073/pnas.1014798108
- 917 Kok, J. F., Adebiyi, A. A., Albani, S., Balkanski, Y., Checa-Garcia, R., Chin, M., ...
 918 Wan, J. S. (2021, May). Contribution of the world's main dust source regions
 919 to the global cycle of desert dust. *Atmospheric Chemistry and Physics*, 21(10),
 920 8169–8193. Retrieved 2022-07-18, from <https://acp.copernicus.org/articles/21/8169/2021/> (Publisher: Copernicus GmbH) doi: 10.5194/acp-21-8169-2021
- 921 Kok, J. F., Mahowald, N. M., Fratini, G., Gillies, J. A., Ishizuka, M., Leys, J. F.,
 922 ... Zobeck, T. M. (2014). An improved dust emission model – part 1: Model
 923 description and comparison against measurements. *Atmospheric Chemistry and
 924 Physics*, 14(23), 13023–13041. Retrieved from <https://acp.copernicus.org/articles/14/13023/2014/> doi: 10.5194/acp-14-13023-2014
- 925 Kok, J. F., Storelvmo, T., Karydis, V. A., Adebiyi, A. A., Mahowald, N. M., Evan,
 926 A. T., ... Leung, D. M. (2023, January). Mineral dust aerosol impacts on
 927 global climate and climate change. *Nature Reviews Earth & Environment*, 1–
 928 16. Retrieved 2023-01-26, from <https://www.nature.com/articles/s43017-022-00379-5> (Publisher: Nature Publishing Group) doi: 10.1038/s43017-022-00379-5
- 929 Kylling, A., Groot Zwaftink, C. D., & Stohl, A. (2018). Mineral dust instantaneous
 930 radiative forcing in the arctic. *Geophysical Research Letters*, 45(9), 4290–4298.
 931 Retrieved from <https://agupubs.onlinelibrary.wiley.com/doi/abs/10.1029/2018GL077346> doi: <https://doi.org/10.1029/2018GL077346>
- 932 Li, L., Mahowald, N. M., Miller, R. L., Pérez García-Pando, C., Klose, M., Hamilton,
 933 D. S., ... Thompson, D. R. (2021, March). Quantifying the range of
 934 the dust direct radiative effect due to source mineralogy uncertainty. *Atmo-*
 935 *spheric Chemistry and Physics*, 21(5), 3973–4005. Retrieved 2023-10-18, from
 936 <https://acp.copernicus.org/articles/21/3973/2021/> (Publisher: Copernicus GmbH) doi: 10.5194/acp-21-3973-2021
- 937 Liu, H., Liu, X., & Dong, B. (2018). Influence of central siberian snow-albedo
 938 feedback on the spring east asian dust cycle and connection with the preced-
 939 ing winter arctic oscillation. *Journal of Geophysical Research: Atmospheres*,
 940 123(23), 13,368–13,385. Retrieved from <https://agupubs.onlinelibrary.wiley.com/doi/abs/10.1029/2018JD029385> doi: <https://doi.org/10.1029/2018JD029385>
- 941 Liu, J., Wu, D., Liu, G., Mao, R., Chen, S., Ji, M., ... others (2020). Impact of
 942 arctic amplification on declining spring dust events in east asia. *Climate Dy-*
 943 *namics*, 54(3), 1913–1935.
- 944 Lu, H., Wang, X., & Li, L. (2010, January). Aeolian sediment evidence that global
 945 cooling has driven late Cenozoic stepwise aridification in central Asia. *Geologi-*
 946 *cal Society, London, Special Publications*, 342(1), 29–44. Retrieved 2023-10-16,
 947 from <https://www.lyellcollection.org/doi/abs/10.1144/sp342.4> (Pub-
 948 lisher: The Geological Society of London) doi: 10.1144/SP342.4
- 949 Maher, B. A. (2016). Palaeoclimatic records of the loess/palaeosol sequences of
 950 the Chinese Loess Plateau. *Quaternary Science Reviews*, 154, 23–84. Re-
 951 tried from <https://www.sciencedirect.com/science/article/pii/S0277379116302761> doi: <https://doi.org/10.1016/j.quascirev.2016.08.004>
- 952 Mao, R., Ho, C.-H., Shao, Y., Gong, D.-Y., & Kim, J. (2011). Influence of arctic
 953 oscillation on dust activity over northeast asia. *Atmospheric environment*,
 954 45(2), 326–337.
- 955 Martin, J. H. (1990). Glacial-interglacial CO₂ change: The Iron Hypothe-
 956 sis. *Paleoceanography*, 5(1), 1–13. Retrieved 2023-10-16, from <https://onlinelibrary.wiley.com/doi/abs/10.1029/PA005i001p00001> (_eprint:
 957 <https://agupubs.onlinelibrary.wiley.com/doi/pdf/10.1029/PA005i001p00001>)
- 958

- 969 doi: 10.1029/PA005i001p00001
- 970 Miao, X., Sun, Y., Lu, H., & Mason, J. (2004). Spatial pattern of grain size in the
971 late pliocene ‘red clay’deposits (north china) indicates transport by low-level
972 northerly winds. *Palaeogeography, Palaeoclimatology, Palaeoecology*, 206(1-2),
973 149–155.
- 974 Nie, J., Pullen, A., Garzione, C. N., Peng, W., & Wang, Z. (2018). Pre-quaternary
975 decoupling between asian aridification and high dust accumulation rates. *Sci-
976 ence Advances*, 4(2), eaao6977. Retrieved from <https://www.science.org/doi/abs/10.1126/sciadv.aa06977> doi: 10.1126/sciadv.aa06977
- 977 Nie, J., Stevens, T., Rittner, M., Stockli, D., Garzanti, E., Limonta, M., ... Pan,
978 B. (2015, October). Loess Plateau storage of Northeastern Tibetan Plateau-
979 derived Yellow River sediment. *Nature Communications*, 6(1), 8511. Retrieved
980 2023-10-16, from <https://www.nature.com/articles/ncomms9511> (Number:
981 1 Publisher: Nature Publishing Group) doi: 10.1038/ncomms9511
- 982 Peng, F., Nie, J., Stevens, T., & Pan, B. (2022). Decoupled Chinese
983 Loess Plateau Dust Deposition and Asian Aridification at Millen-
984 nial and Tens of Millennial Timescales. *Geophysical Research Let-
985 ters*, 49(20), e2022GL099338. Retrieved 2023-10-29, from <https://onlinelibrary.wiley.com/doi/abs/10.1029/2022GL099338> (_eprint:
986 <https://agupubs.onlinelibrary.wiley.com/doi/pdf/10.1029/2022GL099338>) doi:
987 10.1029/2022GL099338
- 988 Peng, W., Zhang, H., Pullen, A., Li, M., Pan, B., Xiao, W., & Nie, J. (2023, March).
989 Stepwise increased spatial provenance contrast on the Chinese Loess Plateau
990 over late Miocene-Pleistocene. *Communications Earth & Environment*, 4(1),
991 1–9. Retrieved 2023-09-10, from <https://www.nature.com/articles/s43247-023-00721-9> (Number: 1 Publisher: Nature Publishing Group) doi: 10
992 .1038/s43247-023-00721-9
- 993 Pisso, I., Sollum, E., Grythe, H., Kristiansen, N. I., Cassiani, M., Eckhardt, S., ...
994 Stohl, A. (2019). The lagrangian particle dispersion model flexpart version
995 10.4. *Geoscientific Model Development*, 12(12), 4955–4997. Retrieved from
996 <https://gmd.copernicus.org/articles/12/4955/2019/> doi: 10.5194/gmd-12-4955-2019
- 997 Porter, S. C. (2001). Chinese loess record of monsoon climate during the last
998 glacial-interglacial cycle. *Earth-Science Reviews*, 54(1), 115–128. Re-
999 tried from <https://www.sciencedirect.com/science/article/pii/S0012825201000435> doi: [https://doi.org/10.1016/S0012-8252\(01\)00043-5](https://doi.org/10.1016/S0012-8252(01)00043-5)
- 1000 Posselt, R., & Lohmann, U. (2008, July). Influence of Giant CCN on warm rain pro-
1001 cesses in the ECHAM5 GCM. *Atmospheric Chemistry and Physics*, 8(14),
1002 3769–3788. Retrieved 2023-10-06, from <https://acp.copernicus.org/articles/8/3769/2008/> (Publisher: Copernicus GmbH) doi: 10.5194/acp-8-3769-2008
- 1003 Qiang, X., An, Z., Song, Y., Chang, H., Sun, Y., Liu, W., ... others (2011). New
1004 eolian red clay sequence on the western chinese loess plateau linked to onset of
1005 asian desertification about 25 ma ago. *Science China Earth Sciences*, 54(1),
1006 136–144.
- 1007 Ren, X., Nie, J., Saylor, J. E., Wang, X., Liu, F., & Horton, B. K. (2020).
1008 Temperature Control on Silicate Weathering Intensity and Evolution of
1009 the Neogene East Asian Summer Monsoon. *Geophysical Research Let-
1010 ters*, 47(15), e2020GL088808. Retrieved 2023-10-13, from <https://onlinelibrary.wiley.com/doi/abs/10.1029/2020GL088808> (_eprint:
1011 <https://agupubs.onlinelibrary.wiley.com/doi/pdf/10.1029/2020GL088808>) doi:
1012 10.1029/2020GL088808
- 1013 Roe, G. (2009, March). On the interpretation of Chinese loess as a paleocli-
1014 mate indicator. *Quaternary Research*, 71(2), 150–161. Retrieved 2023-
1015 10-18, from <https://www.sciencedirect.com/science/article/pii/>

- 1024 S0033589408001154 doi: 10.1016/j.yqres.2008.09.004
- 1025 Ryder, C. L., Marenco, F., Brooke, J. K., Estelles, V., Cotton, R., Formenti, P., ...
 1026 Murray, B. J. (2018, December). Coarse-mode mineral dust size distributions,
 1027 composition and optical properties from AER-D aircraft measurements over
 1028 the tropical eastern Atlantic. *Atmospheric Chemistry and Physics*, 18(23),
 1029 17225–17257. Retrieved 2023-09-09, from <https://acp.copernicus.org/articles/18/17225/2018/> (Publisher: Copernicus GmbH) doi: 10.5194/acp-18-17225-2018
- 1030 Sagoo, N., & Storelvmo, T. (2017). Testing the sensitivity of past cli-
 1031 mates to the indirect effects of dust. *Geophysical Research Let-
 1032 ters*, 44(11), 5807–5817. Retrieved 2022-07-18, from <https://onlinelibrary.wiley.com/doi/abs/10.1002/2017GL072584> (_eprint:
 1033 <https://onlinelibrary.wiley.com/doi/pdf/10.1002/2017GL072584>) doi: 10.1002/
 1034 2017GL072584
- 1035 Sakai, K., & Kawamura, R. (2009). Remote response of the east asian winter
 1036 monsoon to tropical forcing related to el niño–southern oscillation. *Journal
 1037 of Geophysical Research: Atmospheres*, 114(D6). Retrieved from <https://agupubs.onlinelibrary.wiley.com/doi/abs/10.1029/2008JD010824> doi:
 1038 <https://doi.org/10.1029/2008JD010824>
- 1039 Sarangi, C., Qian, Y., Rittger, K., Ruby Leung, L., Chand, D., Bormann, K. J., &
 1040 Painter, T. H. (2020, NOV). Dust dominates high-altitude snow darkening
 1041 and melt over high-mountain asia. *NATURE CLIMATE CHANGE*, 10(11),
 1042 1045+. doi: 10.1038/s41558-020-00909-3
- 1043 Seibert, P., & Frank, A. (2004). Source-receptor matrix calculation with a la-
 1044 grangian particle dispersion model in backward mode. *Atmospheric Chemistry
 1045 and Physics*, 4(1), 51–63.
- 1046 Shang, Y., Beets, C. J., Tang, H., Prins, M. A., Lahaye, Y., van Elsas, R., ...
 1047 Kaakininen, A. (2016). Variations in the provenance of the late neogene red clay
 1048 deposits in northern china. *Earth and Planetary Science Letters*, 439, 88–100.
- 1049 Shao, Y., & Dong, C. (2006). A review on east asian dust storm climate, modelling
 1050 and monitoring. *Global and Planetary Change*, 52(1-4), 1–22. doi: <https://doi.org/10.1016/j.gloplacha.2006.02.011>
- 1051 Shao, Y., & Lu, H. (2000). A simple expression for wind erosion threshold friction
 1052 velocity. *Journal of Geophysical Research: Atmospheres*, 105(D17), 22437–
 1053 22443.
- 1054 Shao, Y., Wyrwoll, K.-H., Chappell, A., Huang, J., Lin, Z., McTainsh, G. H., ...
 1055 Yoon, S. (2011). Dust cycle: An emerging core theme in earth system science.
 1056 *Aeolian Research*, 2(4), 181–204.
- 1057 Shi, Z., & Liu, X. (2011). Distinguishing the provenance of fine-grained eolian dust
 1058 over the chinese loess plateau from a modelling perspective. *Tellus B: Chemi-
 1059 cal and Physical Meteorology*, 63(5), 959–970.
- 1060 Stevens, T., Buylaert, J.-P., Thiel, C., Újvári, G., Yi, S., Murray, A. S., ... Lu, H.
 1061 (2018, March). Ice-volume-forced erosion of the Chinese Loess Plateau global
 1062 Quaternary stratotype site. *Nature Communications*, 9(1), 983. Retrieved
 1063 2023-11-14, from <https://www.nature.com/articles/s41467-018-03329-2>
 1064 (Number: 1 Publisher: Nature Publishing Group) doi: 10.1038/s41467-018
 1065 -03329-2
- 1066 Stevens, T., Carter, A., Watson, T. P., Vermeesch, P., Andò, S., Bird, A. F., ...
 1067 Sevastjanova, I. (2013, October). Genetic linkage between the Yellow River,
 1068 the Mu Us desert and the Chinese Loess Plateau. *Quaternary Science Reviews*,
 1069 78, 355–368. Retrieved 2023-09-10, from <https://www.sciencedirect.com/science/article/pii/S0277379112005343> doi: 10.1016/j.quascirev.2012.11
 1070 .032
- 1071 Stevens, T., Thomas, D. S. G., Armitage, S. J., Lunn, H. R., & Lu, H. (2007, JAN).
 1072 Reinterpreting climate proxy records from late quaternary chinese loess: A de-
 1073

- tailed osl investigation. *EARTH-SCIENCE REVIEWS*, 80(1-2), 111-136. doi: 10.1016/j.earscirev.2006.09.001
- Stohl, A., Forster, C., Frank, A., Seibert, P., & Wotawa, G. (2005). Technical note: The lagrangian particle dispersion model flexpart version 6.2. *Atmospheric Chemistry and Physics*, 5(9), 2461–2474. Retrieved from <https://acp.copernicus.org/articles/5/2461/2005/> doi: 10.5194/acp-5-2461-2005
- Storelvmo, T. (2017). Aerosol effects on climate via mixed-phase and ice clouds. In R. Jeanloz & K. Freeman (Eds.), *Annual review of earth and planetary sciences*, vol 45 (Vol. 45, p. 199-222). doi: 10.1146/annurev-earth-060115-012240
- Sun, D. (2004). Monsoon and westerly circulation changes recorded in the late Cenozoic aeolian sequences of Northern China. *Global and Planetary Change*, 41(1). doi: 10.1016/j.gloplacha.2003.11.001
- Sun, D., Su, R., Bloemendal, J., & Lu, H. (2008, 7). Grain-size and accumulation rate records from late cenozoic aeolian sequences in northern china: Implications for variations in the east asian winter monsoon and westerly atmospheric circulation. *Palaeogeography, Palaeoclimatology, Palaeoecology*, 264, 39-53. doi: 10.1016/J.PALAEO.2008.03.011
- Sun, J., Zhang, M., & Liu, T. (2001). Spatial and temporal characteristics of dust storms in china and its surrounding regions, 1960–1999: Relations to source area and climate. *Journal of Geophysical Research: Atmospheres*, 106(D10), 10325–10333.
- Sun, Y., Yan, Y., Nie, J., Li, G., Shi, Z., Qiang, X., ... An, Z. (2020). Source-to-sink fluctuations of Asian aeolian deposits since the late Oligocene. *Earth-Science Reviews*, 200. doi: 10.1016/j.earscirev.2019.102963
- Tang, H., Haugvaldstad, O. W., Stordal, F., Bi, J., Groot Zwaftink, C. D., Grythe, H., ... Kaakinen, A. (2023). Modelling the 2021 East Asia super dust storm using FLEXPART and FLEXDUST and its comparison with re-analyses and observations. *Frontiers in Environmental Science*, 10. Retrieved 2023-02-08, from <https://www.frontiersin.org/articles/10.3389/fenvs.2022.1013875>
- Thompson, D. W., & Wallace, J. M. (1998). The arctic oscillation signature in the wintertime geopotential height and temperature fields. *Geophysical research letters*, 25(9), 1297–1300.
- Tipka, A., Haimberger, L., & Seibert, P. (2020, November). Flex_extract v7.1.2 – a software package to retrieve and prepare ECMWF data for use in FLEXPART. *Geoscientific Model Development*, 13(11), 5277–5310. Retrieved 2021-01-25, from <https://gmd.copernicus.org/articles/13/5277/2020/> (Publisher: Copernicus GmbH) doi: <https://doi.org/10.5194/gmd-13-5277-2020>
- Tsoar, H., & Pye, K. (1987). Dust transport and the question of desert loess formation. *Sedimentology*, 34(1), 139–153. Retrieved 2023-10-16, from <https://onlinelibrary.wiley.com/doi/abs/10.1111/j.1365-3091.1987.tb00566.x> (_eprint: <https://onlinelibrary.wiley.com/doi/pdf/10.1111/j.1365-3091.1987.tb00566.x>) doi: 10.1111/j.1365-3091.1987.tb00566.x
- Van Der Does, M., Knippertz, P., Zschenderlein, P., Harrison, R. G., & Stuut, J.-B. W. (2018). The mysterious long-range transport of giant mineral dust particles. *Science advances*, 4(12), eaau2768.
- Varga, G., Dagsson-Waldhauserová, P., Gresina, F., & Helgadottir, A. (2021, June). Saharan dust and giant quartz particle transport towards Iceland. *Scientific Reports*, 11(1), 11891. Retrieved 2023-10-16, from <https://www.nature.com/articles/s41598-021-91481-z> (Number: 1 Publisher: Nature Publishing Group) doi: 10.1038/s41598-021-91481-z
- Wang, L., & Chen, W. (2010, July). How well do existing indices measure the strength of the East Asian winter monsoon? *Advances in Atmospheric Sciences*, 27(4), 855–870. Retrieved from <https://doi.org/10.1007/s00376>

- 1134 -009-9094-3 doi: 10.1007/s00376-009-9094-3
- 1135 Wittmann, M., Groot Zwaftink, C. D., Steffensen Schmidt, L., Guð mundsson, S.,
1136 Pálsson, F., Arnalds, O., ... Stohl, A. (2017). Impact of dust deposition on
1137 the albedo of vatnajökull ice cap, iceland. *The Cryosphere*, 11(2), 741–754.
1138 Retrieved from <https://tc.copernicus.org/articles/11/741/2017/> doi:
1139 10.5194/tc-11-741-2017
- 1140 Yang, X., Zeng, G., Zhang, G., & Li, Z. (2020). Interdecadal variation of winter
1141 cold surge path in east asia and its relationship with arctic sea ice. *Journal
1142 of Climate*, 33(11), 4907 - 4925. Retrieved from <https://journals.ametsoc.org/view/journals/clim/33/11/jcli-d-19-0751.1.xml> doi: <https://doi.org/10.1175/JCLI-D-19-0751.1>
- 1145 Yao, J., Chen, Y., Yu, X., Zhao, Y., Guan, X., & Yang, L. (2020, MAY 15). Evalu-
1146 ation of multiple gridded precipitation datasets for the arid region of northwest-
1147 ern china. *ATMOSPHERIC RESEARCH*, 236. doi: 10.1016/j.atmosres.2019
1148 .104818
- 1149 Yao, W., Che, H., Gui, K., Wang, Y., & Zhang, X. (2020). Can merra-2 reanalysis
1150 data reproduce the three-dimensional evolution characteristics of a typical dust
1151 process in east asia? a case study of the dust event in may 2017. *Remote Sens-
1152 ing*, 12(6). Retrieved from <https://www.mdpi.com/2072-4292/12/6/902> doi:
1153 10.3390/rs12060902
- 1154 Yu, H., Chin, M., Yuan, T., Bian, H., Remer, L. A., Prospero, J. M., ... others
1155 (2015). The fertilizing role of african dust in the amazon rainforest: A first
1156 multiyear assessment based on data from cloud-aerosol lidar and infrared
1157 pathfinder satellite observations. *Geophysical Research Letters*, 42(6), 1984–
1158 1991.
- 1159 Zamora, L. M., Kahn, R. A., Evangelou, N., Groot Zwaftink, C. D., & Huebert,
1160 K. B. (2022, September). Comparisons between the distributions of dust
1161 and combustion aerosols in MERRA-2, FLEXPART, and CALIPSO and
1162 implications for deposition freezing over wintertime Siberia. *Atmospheric
1163 Chemistry and Physics*, 22(18), 12269–12285. Retrieved 2023-10-31, from
1164 <https://acp.copernicus.org/articles/22/12269/2022/> (Publisher:
1165 Copernicus GmbH) doi: 10.5194/acp-22-12269-2022
- 1166 Zhang, H., Lu, H., He, J., Xie, W., Wang, H., Zhang, H., ... Li, G. (2022). Large-
1167 number detrital zircon U-Pb ages reveal global cooling caused the formation of
1168 the Chinese Loess Plateau during Late Miocene. *Science Advances*, 8(41). doi:
1169 10.1126/sciadv.abq2007
- 1170 Zhang, H., Nie, J., Liu, X., Pullen, A., Li, G., Peng, W., & Zhang, H. (2021,
1171 June). Spatially variable provenance of the Chinese Loess Plateau. *Ge-
1172 ology*, 49(10), 1155–1159. Retrieved from <https://doi.org/10.1130/G48867.1> (_eprint: <https://pubs.geoscienceworld.org/gsa/geology/article-pdf/49/10/1155/5413499/g48867.1.pdf>) doi: 10.1130/G48867.1
- 1175 Zhang, X., Sharratt, B., Lei, J.-Q., Wu, C.-L., Zhang, J., Zhao, C., ... Hao, J.-
1176 Q. (2019, July). Parameterization schemes on dust deposition in north-
1177 west China: Model validation and implications for the global dust cycle. *At-
1178 mospheric Environment*, 209, 1–13. Retrieved 2023-09-25, from <https://www.sciencedirect.com/science/article/pii/S1352231019302328> doi:
1179 10.1016/j.atmosenv.2019.04.017
- 1181 Zhao, A., Ryder, C. L., & Wilcox, L. J. (2022). How well do the cmip6 models simu-
1182 late dust aerosols? *Atmospheric Chemistry and Physics*, 22(3), 2095–2119. Re-
1183 trievied from <https://acp.copernicus.org/articles/22/2095/2022/> doi:
1184 10.5194/acp-22-2095-2022